Tectonics

RESEARCH ARTICLE

10.1029/2021TC006786

High-Resolution Seismic Profiling in the Hanging Wall of the Southern Fault Section Ruptured During the 2016 M_w 6.5 Central Italy Earthquake

Fabio Villani[1], Stefano Maraio[1,2], Pier Paolo Bruno[3], Luigi Improta[1], Kieran Wood[4], Stefano Pucci[1], Riccardo Civico[1], Vincenzo Sapia[1], Paolo Marco De Martini[1], Carlo Alberto Brunori[1], Carlo Doglioni[1], and Daniela Pantosti[1]

[1]Istituto Nazionale di Geofisica e Vulcanologia, Rome, Italy, [2]Centro di Geotecnologie, Università di Siena, San Giovanni Valdarno, Italy, [3]Università degli Studi di Napoli Federico II, Napoli, Italy, [4]Horizon Union LDT, Derby, UK

Abstract The Vettore–Bove normal fault system in central Italy ruptured during the 2016 M_W 6.5 Norcia earthquake causing extensive surface faulting. At the Pian Grande di Castelluccio hanging wall basin, along the southern section of the fault ruptured during the M_W 6.5 mainshock, we performed a high-resolution seismic reflection/refraction experiment aimed at (a) imaging the shallow pattern of the fault system, and (b) reconstructing the architecture of the continental infill. We collected three profiles for a total length of ~8 km. We used a reflection processing flow and non-linear refraction tomography to obtain migrated stack sections and P-wave velocity images resolved down to the depth of the pre-Quaternary substratum. The main profile in the northern part of the basin crosses the westernmost splays of the ruptured fault zone striking N150°–170°. Seismic imaging unravels a ~1 km-wide fault zone comprising three W-throwing splays and subsidiary faults, which affect the continental infill and produce a minimum aggregate Quaternary throw of ~400 ± 100 m. Recent deformation is localized in this part of the surveyed fault section, attesting active displacement accumulation of the Vettore–Bove fault system. The other profiles in the central-southern part of the basin show additional faults, likely striking N20°–40° and which concurred to generate a ~500 m-deep depocenter. These faults were mostly active during an early extensional phase; however, one of them likely displaces shallow layers with a throw close to the resolution limit of seismic data (<10 m), suggesting activity in the Late Pleistocene.

Key Points:

- Three high resolution seismic profiles image the hanging wall of southern part of the 2016 M_W 6.5 central Italy earthquake fault zone
- The surveyed ~1 km-wide hidden fault section displays three active W-dipping splays with a minimum aggregate Quaternary throw of ~400 m
- P-wave velocity tomographic images and migrated sections depict a ~500 m-deep Quaternary depocenter in the earthquake fault hanging wall

Supporting Information:

Supporting Information may be found in the online version of this article.

Correspondence to:

F. Villani,
fabio.villani@ingv.it

Citation:

Villani, F., Maraio, S., Bruno, P. P., Improta, L., Wood, K., Pucci, S., et al. (2021). High-resolution seismic profiling in the hanging wall of the southern fault section ruptured during the 2016 M_w 6.5 central Italy earthquake. *Tectonics*, *40*, e2021TC006786. https://doi.org/10.1029/2021TC006786

Received 26 FEB 2021
Accepted 13 AUG 2021

1. Introduction

In regions of active extension, normal faulting over timescales of 10^4–10^6 years generates extensional hanging wall basins that entrap sediments mainly conveyed from the uplifted footwall blocks (e.g., Burbank & Anderson, 2011; Meyer et al., 2002; Nixon, Bull, & Sanderson, 2014; Silva et al., 2003). Fault growth controls the first-order geometry and size of those basins, whereas the erosional-depositional systems react to this tectonic forcing with different amount and styles of clastic supply and alluvial sedimentation (Bull, 2009; Gallen & Wegmann, 2017; Gawthorpe & Leeder, 2000; Mustard, 1991; Whittaker et al., 2007). Thus, the basins geometry, their sedimentary record and syn-rift depositional architecture provide keys to the amount and pattern of displacement of the major border faults (Manighetti et al., 2001; Mouslopoulou et al., 2009; Nicol et al., 1997, 2010). In this regard, seismic investigations of fault-controlled basins promoted significant advances in understanding the evolution of normal fault-systems at different scales (e.g., Morley, 1999; Nixon, Sanderson, et al., 2014; Reeve et al., 2015; Taylor et al., 2004). High-resolution seismic profiling can define the location and geometry of subsurface faults (Catchings et al., 2008; Everett, 2013; Pratt et al., 1997), and provide key constraints on fault activity through the analysis of the subsurface stratigraphy (e.g., Brocher et al., 1993; Bruno et al., 2013, 2019; Osagiede et al., 2014; Stephenson et al., 1993, 2012, 2013).

The central Apennines (Italy; Figure 1a) is a region of active normal faulting. This fold-and-thrust belt is mostly made of a sedimentary multi-layer (Carminati et al., 2012; Doglioni, 1991, Doglioni et al., 1998; Vai & Martini, 2001) affected by Mesozoic-Tertiary poly-phase tectonics before Miocene thrusting and shortening (e.g., Calamita et al., 2000, 2009). Since the Plio-Quaternary, post-orogenic extension due to slab roll-back of the subducting Adriatic lithosphere (Carminati et al., 2020; Devoti et al., 2008; van Hinsbergen et al., 2014), generated a network of generally NW-trending normal faults organized in ~15–30 km-long

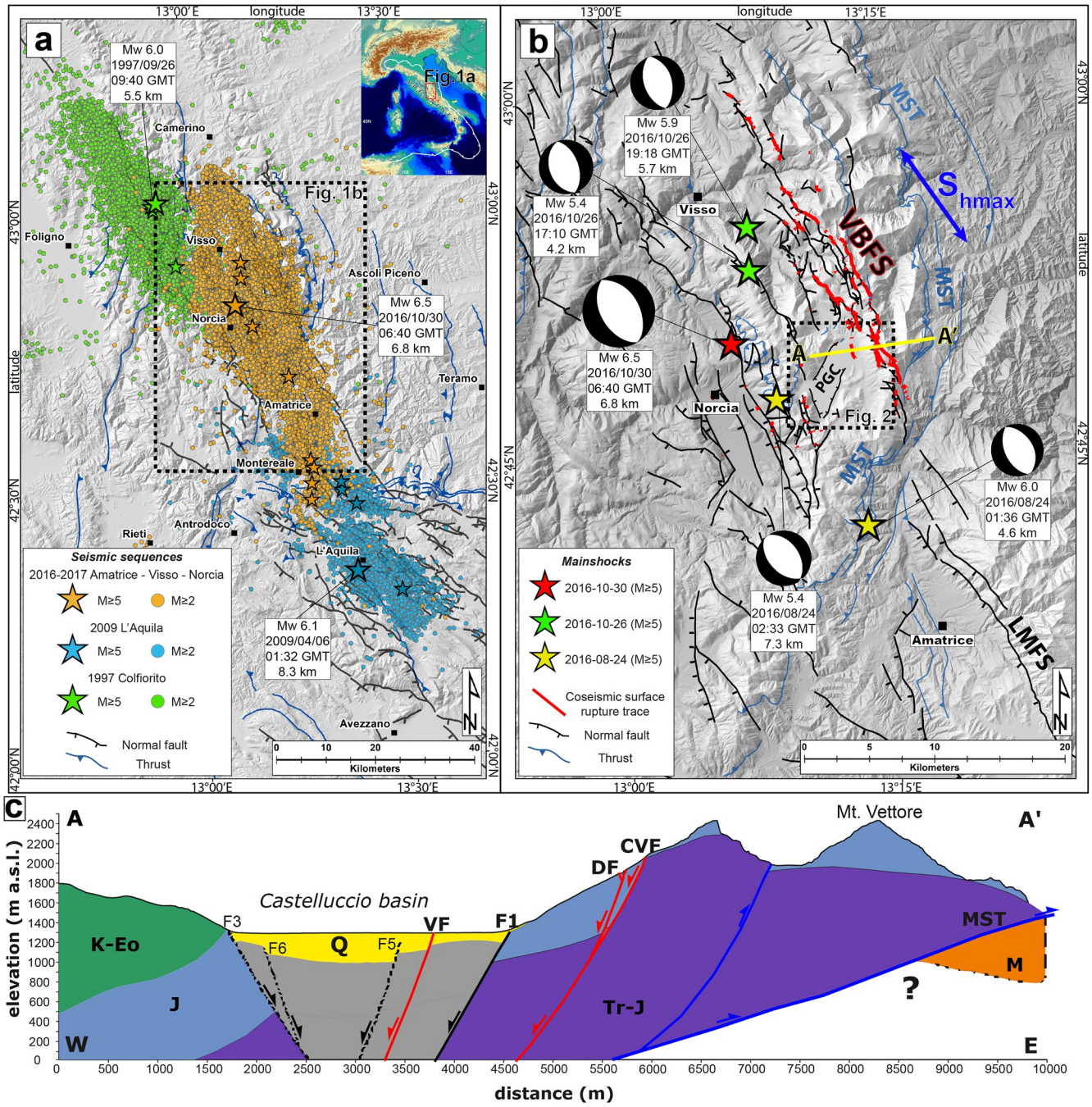

Figure 1. Seismotectonic map of the central Apennines with simplified geological cross-section across the 30 October 2016 M_w 6.5 earthquake fault. (a) Location map of the three main seismic sequences since 1997 in central Italy and their aftershocks (stars indicate M5+ events). The inset shows location of the Apennines. (b) Detailed map of the study area, with main normal faults (black lines; VBFS: Vettore–Bove fault-system), principal thrusts (blue lines, including the Mts. Sibillini Thrust (MST)), the trace of the 2016 coseismic surface ruptures (in red; Civico et al., 2018) and focal mechanisms of the mainshocks of the Amatrice-Visso-Norcia sequence. The blue arrow indicates the direction of the maximum horizontal stress SH_{max} (modified after: Villani et al., 2019). The dashed black rectangle encloses the Castelluccio basin (PGC) and the survey area shown in Figure 2. (c) Schematic geological cross-section A-A′ (based on the low-resolution 1-D and 2-D geophysical data by Villani et al., 2019). Red faults are splays of the Vettore–Bove fault-system that ruptured the surface during the 2016 M_W 6.5 mainshock. Tr-J: Trias–Early Jurassic shallow-water carbonates; (j) Jurassic pelagic carbonates; K-Eo: Cretaceous-Eocene pelagic carbonates; M: Miocene flysch; Q: Quaternary infill. The pre-Quaternary substratum beneath the Castelluccio basin is undifferentiated (gray). For the meaning of fault labels, refer to the main text.

and over-stepping systems (Boncio et al., 2004; Cowie & Roberts, 2001; Cowie et al., 2017; Galadini & Galli, 2000; Figure 1a). These active normal faults display pervasive segmentation, mostly due to geometrical complexities and structural heterogeneities, locally influenced by re-activation of inherited faults (e.g., Pizzi & Galadini, 2009; Tavarnelli, 1999).

In the past 24 years, three major seismic sequences broke a >100 km-long portion of this normal fault network, with mainshocks of M_W 6+ (Figure 1a): 1997 Colfiorito; 2009 L'Aquila; 2016–2017 Amatrice-Visso-Norcia (e.g., Michele et al., 2020 and references therein). In this region, the largest active faults exhibit slip rates generally <1 mm/yr (Benedetti et al., 2013; Galli et al., 2008), and altogether they concur to accommodate regional extension rates of ~1–3 mm/yr (D'Agostino et al., 2008, 2011; Devoti et al., 2011, 2017; Faure Walker et al., 2010).

The active normal fault network in the central Apennines generated several Plio-Quaternary hanging wall basins (Blumetti & Guerrieri, 2007; Bosi et al., 2003; D'Agostino et al., 2001; Geurts et al., 2018; Pizzi et al., 2002). Their subsurface internal architecture, as well as the relations between deep basin structure and long-term faulting, were object of few studies. One main reason is the shortage of high-quality industrial reflection profiles that, with a few exceptions (e.g., Patacca et al., 2008), are generally of fair to low quality in the upper portion of the crust (~0–2 km depth; e.g., Ercoli et al., 2020). For instance, high-resolution seismic profiling of some fault-bounded basins in the 2009 L'Aquila earthquake region (e.g., Improta et al., 2012; Villani, Pucci, et al., 2015; Villani, Tulliani, et al., 2015; Villani, Improta, et al., 2017), enabled to characterize their subsurface structure and evolution in relation to the seismogenic border faults. The investigation depth of such studies is typically ~200–500 m, which partly compensates for the absence and/or poor quality of commercial profiles.

This study deals with the first high-resolution seismic survey of the southern portion of the Vettore–Bove normal fault system, in the Pian Grande di Castelluccio basin (Castelluccio basin hereinafter; Figure 1b). The Vettore–Bove fault-system is the source of the M_W 6.5, 2016 Norcia earthquake, the largest event that hit Italy in the past four decades. Details of the earthquake source and rupture characteristics were subject of several studies (Section 2). This event caused widespread surface faulting (Figure 1) also affecting the northern part of the Castelluccio basin (e.g., Civico et al., 2018; Villani, Civico, et al., 2018). Normal faulting likely promoted internal drainage system, hampering significant fluvial incision of this basin (D'Agostino et al., 2001). This created an ideal setting for seismic imaging, since the subsurface may contain a potentially continuous sedimentary record of Quaternary age.

We collected three high-resolution seismic profiles for a total length of ~8 km (Figure 2). The main profile, to the north, targets the westernmost surface-rupturing strands of the Vettore–Bove fault-system. Prohibitive topographic conditions prevent a survey across the entire ~2 km-wide ruptured fault zone. The investigation extends to the central-southern part of the basin through the other two profiles. By adopting a dense, wide-aperture seismic acquisition geometry (Operto et al., 2004), our imaging strategy combines reflection processing with non-linear multi-scale refraction tomography to produce complementary 2-D migrated stack sections and P-wave velocity models (e.g., Improta & Bruno, 2007).

Our study is twofold. First, we image in detail the fault-zone that ruptured during the 2016 earthquake. Second, we define the internal depositional architecture and structure of the basin down to ~500–600 m. We also obtain key information on the location, geometry, and activity of subsurface faults that were unknown before this study. As a corollary aim, we propose a hypothetical scheme of the Quaternary fault and basin evolution.

2. Background

2.1. The Vettore–Bove Fault System and the 2016 M_W 6.5 Earthquake Rupture

The 2016–2017 sequence ruptured a fault-system for a total length of ~60–70 km (Chiaraluce et al., 2017; Michele et al., 2020), including the Vettore–Bove fault-system in the northwest and the Laga Mts. fault-system (Figure 1b) to the southeast. The M_W 6.5 Norcia mainshock was a complex earthquake characterized by a multi-segment rupture that involved almost the entire ~25 km-long Vettore–Bove fault-system, as well as one or more subsidiary faults with various dips and orientations (e.g., Tan et al., 2021 and references

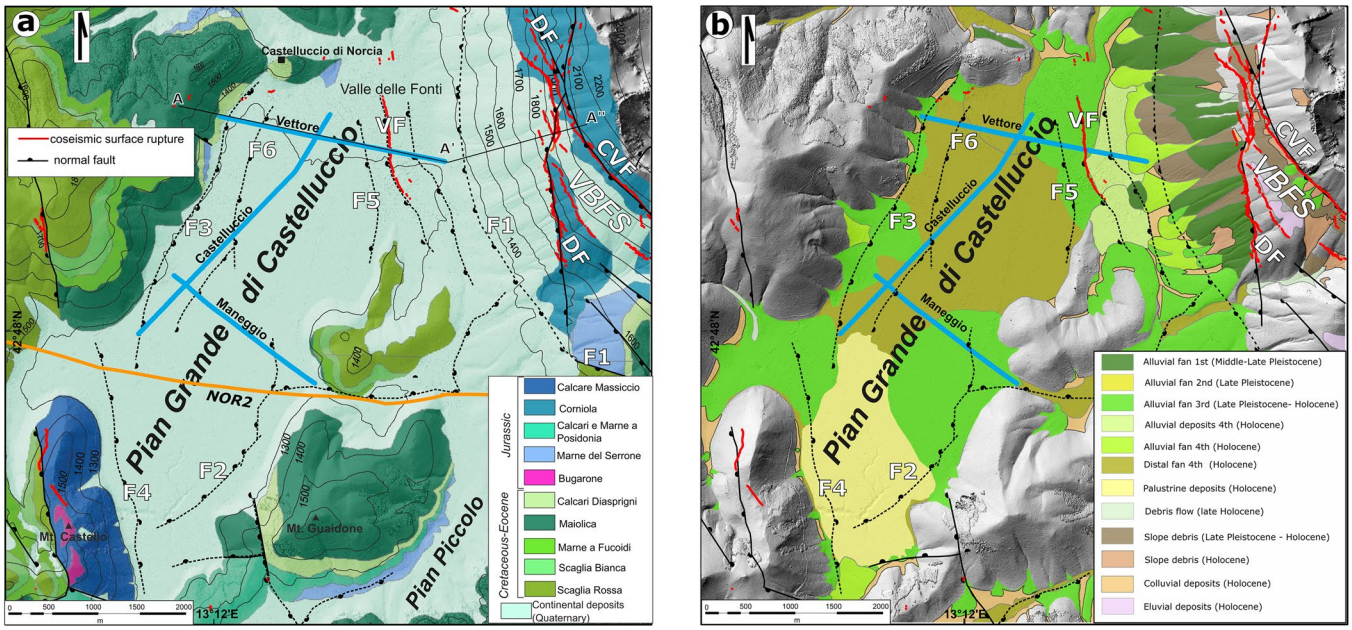

Figure 2. Geological setting of the survey area. (a) Simplified geological map of the Castelluccio basin area. Black lines are faults (modified after Pierantoni et al., 2013). Dashed black lines indicate inferred subsurface faults from previous geophysical studies (F1, F2, F3, F4, F5, F6, and VF, from Villani et al., 2019 and references therein). CVF: Cordone del Vettore Fault. DF: Diagonal Fault. Red lines are coseismic surface ruptures (Civico et al., 2018; Villani, Civico, et al., 2018). Blue lines are the high-resolution seismic profiles described in this work, and the orange line is the portion of commercial profile NOR2 that crosses the basin (Ercoli et al., 2020; Porreca et al., 2018). A–A′–A″ is the trace of the composite interpretative cross-section shown in Figure 10. (b) Map of the main continental deposits in the Castelluccio basin (from this work; see Section 3.2). Shaded relief topography from 0.5 m-grid Pleiades digital elevation model (Delorme et al., 2020).

therein). Several papers described the structural arrangement and recent morphotectonics of the Vettore–Bove fault-system (e.g., Boncio et al., 2004; Calamita & Pizzi, 1992, 1994; Calamita, Pizzi & Roscioni, 1992; Galadini & Galli, 2000; Lavecchia et al., 1994; Pizzi et al., 2002). The latter is composed of five main segments trending ~N150°–170° (except one segment trending ~N340°), ranging in length from ~2 to ~7 km (Villani, Pucci, et al., 2018). To the south, the Vettore–Bove fault-system branches into a ~2 km-wide zone comprising three major diverging segments (Figures 1c and 2) that cross-cut the western slope of Mt. Vettore ridge. From the highest to the lowest one, they are: the ~5 km-long Cordone del Vettore fault (CVF in Figure 1c), located at ~2,000 m *a.s.l.*; the ~3 km-long Diagonal Fault (DF in Figure 1c), located at ~1,400–1,900 m *a.s.l.*; the ~5.5 km-long fault F1, running at the base of the slope (~1,300–1,400 m *a.s.l.*) and bounding the Castelluccio basin to the east. The Cordone del Vettore fault displays a >20 m-high bedrock fault scarp, interpreted as the result of several surface-faulting earthquakes (e.g., Brozzetti et al., 2019; Pizzi et al., 2017; Pucci et al., 2021; Puliti et al., 2020) subsequent to the Last Glacial Maximum (set to 28–26 kyr cal BP by Giraudi, 2015). Fault F1 forms a >1,100 m-high tectonic range front interpreted as expression of long-term displacement; based on the offset of Mesozoic stratigraphic markers, this fault is supposed to have a maximum throw of ~1,200–1,400 m (e.g., Brozzetti et al., 2019; Calamita, Pizzi & Roscioni, 1992; Porreca et al., 2020; Villani et al., 2019; Figure 1c). F1 shows no clear evidence of recent scarplets affecting the alluvial and debris cover, so that the northern-central part of its surface trace is uncertain (e.g., Pierantoni et al., 2013; Figure 2). Repeated surface-rupturing earthquakes recovered from paleoseismic trenches in different sites across the Vettore–Bove fault-system (Cinti et al., 2019; Galadini & Galli, 2003; Galli et al., 2019) attest active faulting in the late Pleistocene–Holocene.

Surface ruptures of the M_W 6.5 Norcia earthquake involved the whole Vettore–Bove fault-system, with dominant normal kinematics (Villani, Pucci, et al., 2018). The along-strike distribution of coseismic surface displacement was asymmetrical, showing a maximum located in the southern part, with local throw reaching ~2 m along the Cordone del Vettore fault (e.g., Brozzetti et al., 2019; Civico et al., 2018; Pizzi et al., 2017; Villani, Civico, et al., 2018, Villani, Pucci, et al., 2018; Wilkinson et al., 2017). Coseismic ruptures occurred also in the northern part of the Castelluccio basin, along the ~1.5 km-long Valle delle Fonti fault (labeled

as VF in Figures 1c, 2a, 6 and 7). The recent activity of the VF fault is attested by paleoseismic evidence of Holocene earthquakes and by a ~3 m-high scarp trending NNW-SSE over a Late Pleistocene-Holocene alluvial fan sequence (Galadini & Galli, 2003). Electrical resistivity tomography (ERT) across the VF fault, points out a local vertical offset of ~5 m affecting the alluvial fan accreted since the Last Glacial Maximum, whereas the inferred total fault throw is ~100–120 m (Villani & Sapia, 2017; Villani et al., 2019).

Coseismic ruptures of the M_W 6.5 Norcia earthquake along the VF fault have a maximum vertical offset of 0.14 m (Cirillo, 2020; Villani, Civico, et al., 2018). These ruptures broke the trench site of Galadini and Galli (2003) (location in Figure 3a). Moreover, while most of the ruptured strands of the Vettore–Bove fault-system cut Mesozoic-Tertiary limestones, the entire trace of the VF fault affects a >100 m-thick package of Quaternary alluvial deposits (Villani & Sapia, 2017; Villani et al., 2019). As such, the VF fault is a premier target, because high-resolution seismic profiling could provide constraints on the fault Quaternary evolution.

2.2. The Castelluccio Basin

The Castelluccio basin (Figure 2) is a ~20 km^2-wide Quaternary intramontane depression with a rhomboid shape due to four major border fault zones (Calamita & Pizzi, 1992, 1994; Calamita, Pizzi & Roscioni, 1992; Coltorti & Farabollini, 1995; Villani et al., 2019): fault F1 (trending ~N150°) to the northeast; fault F2 (trending ~N200°) to the southeast; fault F4 (trending ~N340°) to the south-west; fault F3 (trending ~N20°) to the north-west. The occurrence of faults F2, F3, and F4 is suggested by near-rectilinear border ridges and by the large stratigraphic separation (several hundred meters) occurring between the western and eastern sides of the basin (Calamita, Pizzi & Roscioni, 1992). However, the exact trace of those faults is uncertain, due to the cover of continental deposits (e.g., Pierantoni et al., 2013). Some ERT surveys across limited portions of fault zones F3 and F1 (Figure 3a) confirm their location (Villani et al., 2019). Fault F2, traced by Calamita, Pizzi and Roscioni (1992) and Coltorti and Farabollini (1995) based on geomorphologic considerations, has been recently located close to the base of Mt. Guaidone by Villani et al. (2019) using 1-D resistivity profiles and ambient vibration recordings (Figure 2a). F4 is supposed to bound a Jurassic structural high (Mt. Castello; Figure 2a) and was interpreted as a pre-orogenic extensional fault (e.g., Buttinelli et al., 2021; Calamita, Pizzi & Roscioni, 1992; Pierantoni et al., 2013; Figure 2a).

The substratum outcropping at the basin edges is made of Mesozoic-Tertiary marly limestones and cherts (Figures 1c and 2; Pierantoni et al., 2013). From a seismic imaging perspective, those generally thin-bedded layers have compressional velocity *Vp* ~4,500–5,500 m/s and display internal reflectivity (Bigi et al., 2013; Latorre et al., 2016; Mirabella et al., 2008). However, the only seismic reflection profile crossing the area (labeled as NOR2; trace in Figure 2a) provides poor structural images of the topmost 2 km of the crust, and the Castelluccio basin is not resolved (e.g., Buttinelli et al., 2021; Ercoli et al., 2020; Porreca et al., 2018). In fact, such vintage commercial data, acquired between the 70s and the 90s with both vibroseis and explosive, have low fold coverage (generally <60 traces per common-mid-point) and display overall low signal-to-noise ratio.

So far the only available direct information on the subsurface stratigraphy of the basin is provided by a few boreholes (<100 m-deep; Geomineraria Nazionale, 1963) that indicate the occurrence of alternating gravels, sandy gravels, and clays (Figure 3). Borehole *b5* is <30 m-deep. Boreholes *b2* and *b4* penetrated limestones at −76 and −97 m depth, respectively; however, they are offset from our seismic lines, thus they cannot constrain the top-bedrock in the seismic sections. Villani and Sapia (2017) interpreted the uppermost gravel package in borehole *b5* as Late Pleistocene alluvial fan deposits of the Last Glacial Maximum, whereas the silty-clay layer at depth >15 m in boreholes *b1* and *b4* was correlated with a short-lived lacustrine cycle. Here, we interpret those fine-grained layers as mostly related to distal alluvial deposits. By analogy with the recent palustrine deposits in the swampy southern portion of the basin (Figure 2b), we do not rule out that some silty intervals may have been deposited in local ephemeral ponds (see also Pierantoni et al., 2013).

Previous geophysical surveys suggest that in the northern portion of the basin the infill thickness ranges from ~70 to 100 m close to the western and eastern borders to >300 m in the central part (Villani et al., 2019; Figure 1c).

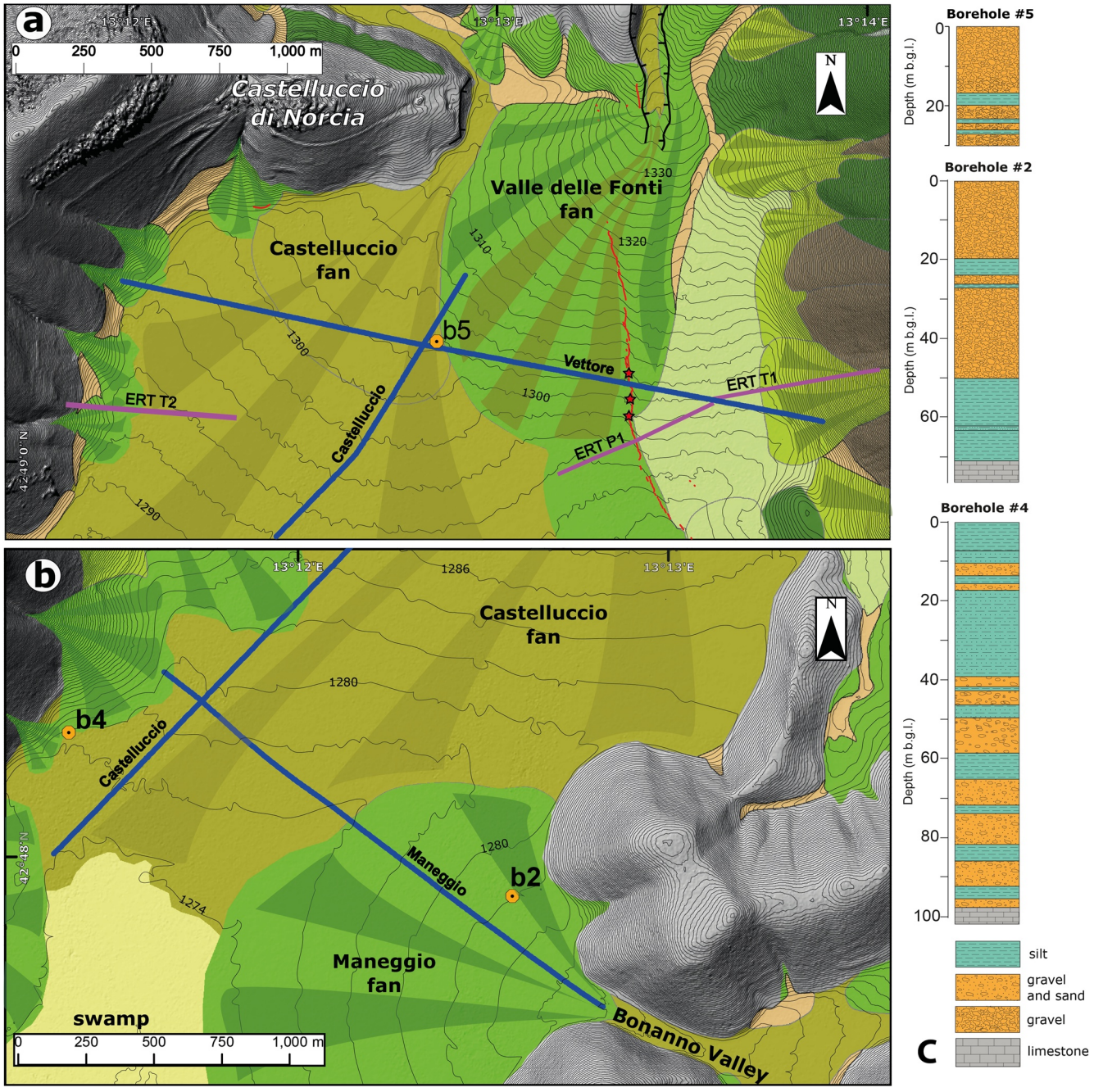

Figure 3. Detailed map of the continental deposits outcropping in the survey area (from this work; see Section 3.2). Blue lines are the three seismic profiles. (a) Location of Vettore Profile and of the northern part of Castelluccio Profile. (b) Survey area of Maneggio Profile and of the southern part of Castelluccio Profile. Pink lines are the traces of the three ERT profiles by Villani and Sapia (2017) and Villani et al. (2019). The main alluvial fan bodies have different green shading according to their inferred relative age (see details in the main text). The trace of the coseismic surface ruptures of the October 30, 2016 M_W 6.5 earthquake (Civico et al., 2018) is in red. The small red stars in panel a indicate trench sites by Galadini and Galli (2003). The dark-shaded lobes superimposed on the fans indicate inferred dominant flow directions and black lines with ticks indicate incision of the apex zones. Topography from Pleiades digital elevation model (Delorme et al., 2020), with contour lines spacing of 2 m. Orange circles indicate boreholes. (c) Stratigraphy of boreholes b2, b4, and b5 used for the lithological interpretation of the shallow portion of the investigated seismic transects (modified after Villani et al., 2019).

3. Materials and Methods

3.1. Seismic Data

During fall 2017, within the Castelluccio basin we acquired three intersecting high-resolution seismic profiles (labeled as Vettore, Maneggio, and Castelluccio; Figure 2), with a 6-ton vibrating source (*MiniVib* IVI®: Industrial Vehicles International). The survey geometry represents the best compromise between geological targets and logistic constraints.

The Vettore Profile, ~N100°-trending and 2,635 m-long, covers the northern part of the Castelluccio basin and crosses nearly at right angle (~80°) the trace of the VF fault. In the eastern part, the profile runs on the steep slope of Mt. Vettore as high as possible (~40 m above the plain) to use the *MiniVib* in safe conditions, and to allow the investigation of the inferred trace of fault F1 (Figures 2 and 3a).

The 2,035 m-long Maneggio Profile trends ~N130° (Figures 2 and 3b). To the east, the profile crosses the subsurface inferred fault F2, which trends oblique with respect to the Vettore–Bove fault-system. To the west, the profile was limited due to logistical problems and the presence of fences and powerlines contaminating seismic signal. Thus, the profile could not reach the base of the long-term cumulative fault scarp F3.

The 3,355 m-long Castelluccio Profile trends ~N30° in the northern section and ~N50° in the central-southern part, following the elongation axis of the Castelluccio basin (Figures 2 and 3).

The adopted acquisition layout consists of an 1,195 m-wide, 240-channel *dense wide-aperture array* (Bruno et al., 2010, 2013; Improta & Bruno, 2007; Operto et al., 2004) deployed with 5 m spacing between the 4.5-Hz vertical sensors connected to a distributed 24-bit Geometrics Geode® acquisition system. The array length is about four times the presumed maximum depth of the basin (~300 m; Figure 1c). This acquisition geometry allows collecting simultaneously: (a) near-vertical and wide-angle reflections generated from deeper interfaces, the last being hardly detectable with shorter geophone spreads, and (b) highly redundant first P-pulses corresponding to shallow direct waves, deep-penetrating turning waves and critical refractions from the basin interior and its substratum, suitable for travel-time tomography (Improta & Bruno, 2007).

Along this array, we recorded at each source point and with a sampling rate of 1 ms, the stack of two, 5–200 Hz, 14.4 s-long linear sweeps from the vibrating source. The listen time after the sweep was 1.6 s (total record length of 16 s). Source move-up was on average 5 m (Table S1). To cover the entire profile length, we walked through the entire 240-channels array, then moved 144 sensors and walked through all 240 channels again, thus leaving a constant overlap of 480 m between adjacent geophone spreads for trace redundancy and increasing fold coverage (up to 160; Figures S2–S4).

From the seismic data set, we hand-picked ~180,000 first-arrival traveltimes to obtain accurate *Vp* models through a multi-scale non-linear tomographic inversion based on a finite-difference eikonal solver (Improta et al., 2002; Podvin & Lecomte, 1991; details in the Text S1). Models are parametrized through a regular grid of velocity nodes. The multi-scale approach consists in gradually increasing the number of nodes during consecutive inversion steps, resulting in an ensemble of models characterized by increasing spatial resolution, achieved at the expense of a loss in resolution depth. Models obtained at intermediate steps of the multi-scale inversion enable the reconstruction of large-scale and deeper features of the subsurface, while models obtained at late steps provide higher resolution images of the shallow structure. To assess resolution of the velocity models, we perform checkerboard tests by applying smooth and small-amplitude velocity perturbations to the grid nodes and then by testing the ability to recover the perturbations after tomographic inversion of synthetic traveltimes (details in Text S1). By considering the nodes spacing and the results of the checkerboard tests, the spatial resolution of the models at the intermediate multi-scale step is ~200 m along x and ~80 m in depth. The investigation depth inferred by back-raytracing plots (e.g., Figures 4 and 5) is ~400–500 m. For each seismic profile, we show a representative best-fit model obtained at the late stage of multi-scale inversion, characterized by investigation depth of ~250–350 m, and which details the shallow features. In this case, the spatial resolution is ~120 m along x and ~60 m in depth (Figures 6, 8 and 9). Such values are consistent with the first Fresnel zone radius evaluated from the dominant wavelength of P-waves in the near offset (e.g., Williamson & Worthington, 1993; details in Text S1). For profile Vettore, we also show a model with spatial resolution of ~60 m along x and ~40 m in depth, which depicts shallow details of the fault zone that ruptured during the M_W 6.5 Norcia earthquake (Figure 7b).

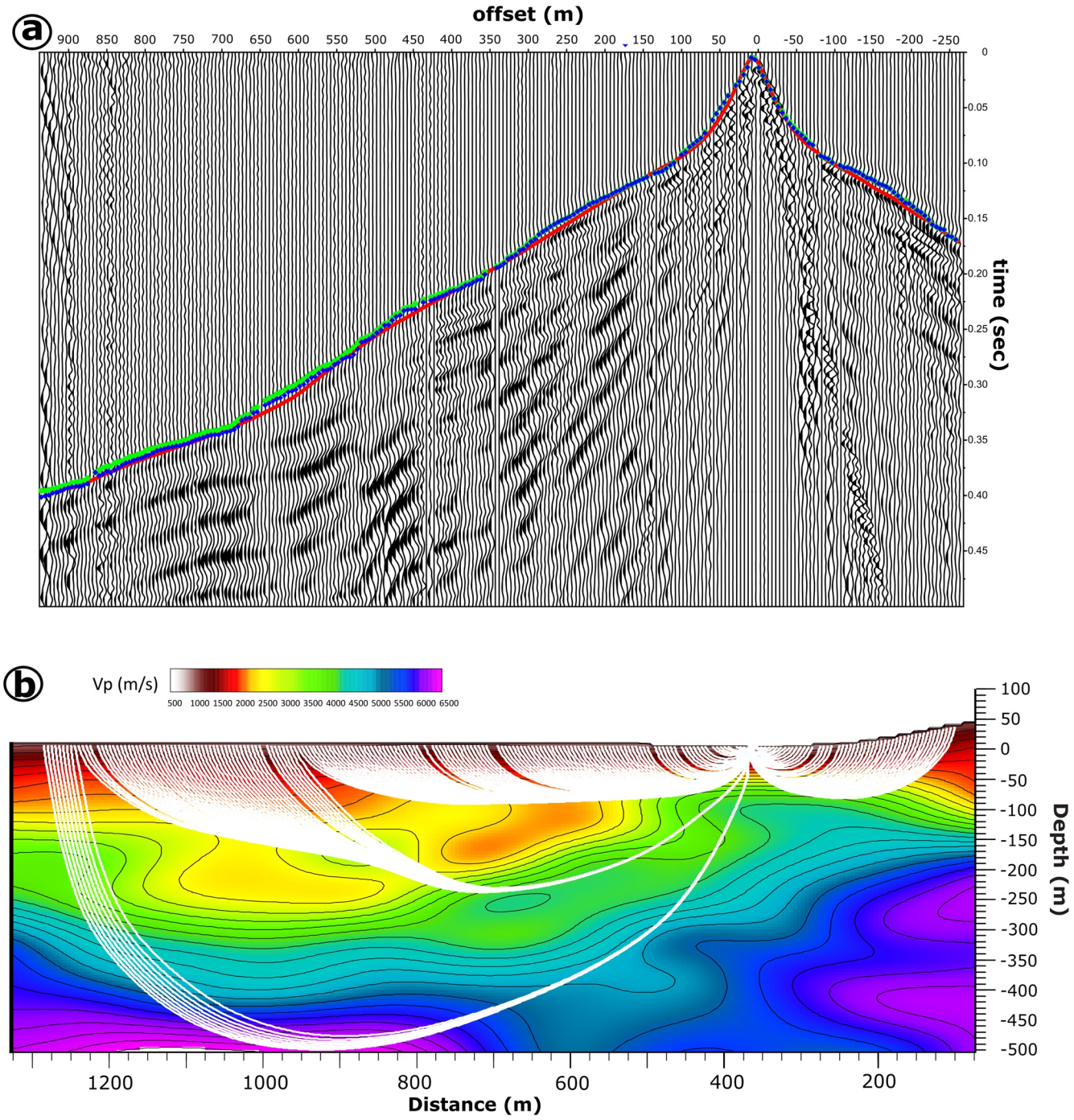

Figure 4. Example of seismic data from Vettore Profile, input traveltimes and tomographic results after the last inversion run. (a) common-shot gather (CSG) 261 (x = 262.5 m; bandpass and 50 Hz notch filter applied) with plot of manual picking (blue and green dots, bracketing the presumed first arrival) and synthetic traveltimes (red curve). (b) Tomographic model (only eastern portion shown) with back-raytracing (thin white lines) for CSG 261.

The reflection processing flow was designed to take advantage of the densely spaced wide-aperture acquisition geometry (Improta & Bruno, 2007). This enables the recording of multi-angle reflections and better focuses the energy reflected from dipping reflectors, such as fault planes and steeply tilted packages expected in the basin subsurface (Bruno, DuRoss, et al., 2017, Bruno, Maraio, et al., 2017; Bruno et al., 2019; Maraio et al., 2018). The preliminary stack sections, obtained with standard common mid point workflow and velocity analysis, were improved with a Common Surface Reflection stack operator (Mann et al., 1999

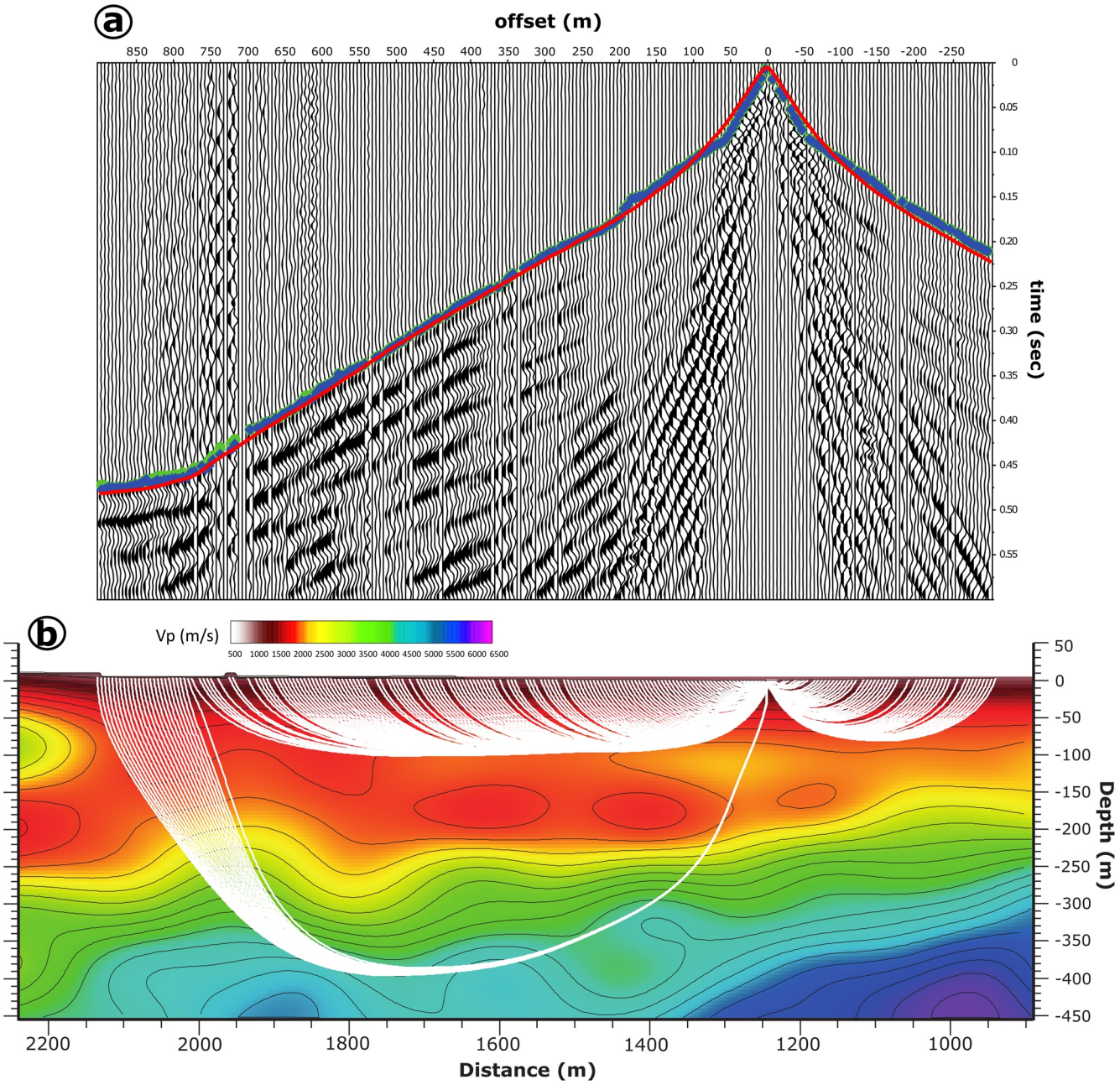

Figure 5. Example of seismic data from Maneggio Profile, input traveltimes and tomographic results after the last inversion run. (a) common-shot gather (CSG) 367 (x = 1,137.5 m; bandpass and 50 Hz notch filter applied) with plot of manual picking (blue and green dots, bracketing the presumed first arrival) and synthetic traveltimes (red curve). (b) Tomographic model (only western portion shown) with back-raytracing (thin white lines) for CSG 367.

and references therein). They were subsequently migrated with an iterative Stolt Migration algorithm (Yilmaz, 2001) and processed with an F-X deconvolution filter (Gulunay, 1986). The final migrated and depth-converted sections are shown in Figures 6–9. Because an exhaustive description is beyond the scope of this study, the workflow and processing parameters are detailed in the Text S2.

3.2. Stratigraphic Data

For the interpretation of the seismic stratigraphy, we take into account available geological and geomorphological maps (e.g., Coltorti & Farabollini, 1995; Pierantoni et al., 2013). In addition, we refined mapping of

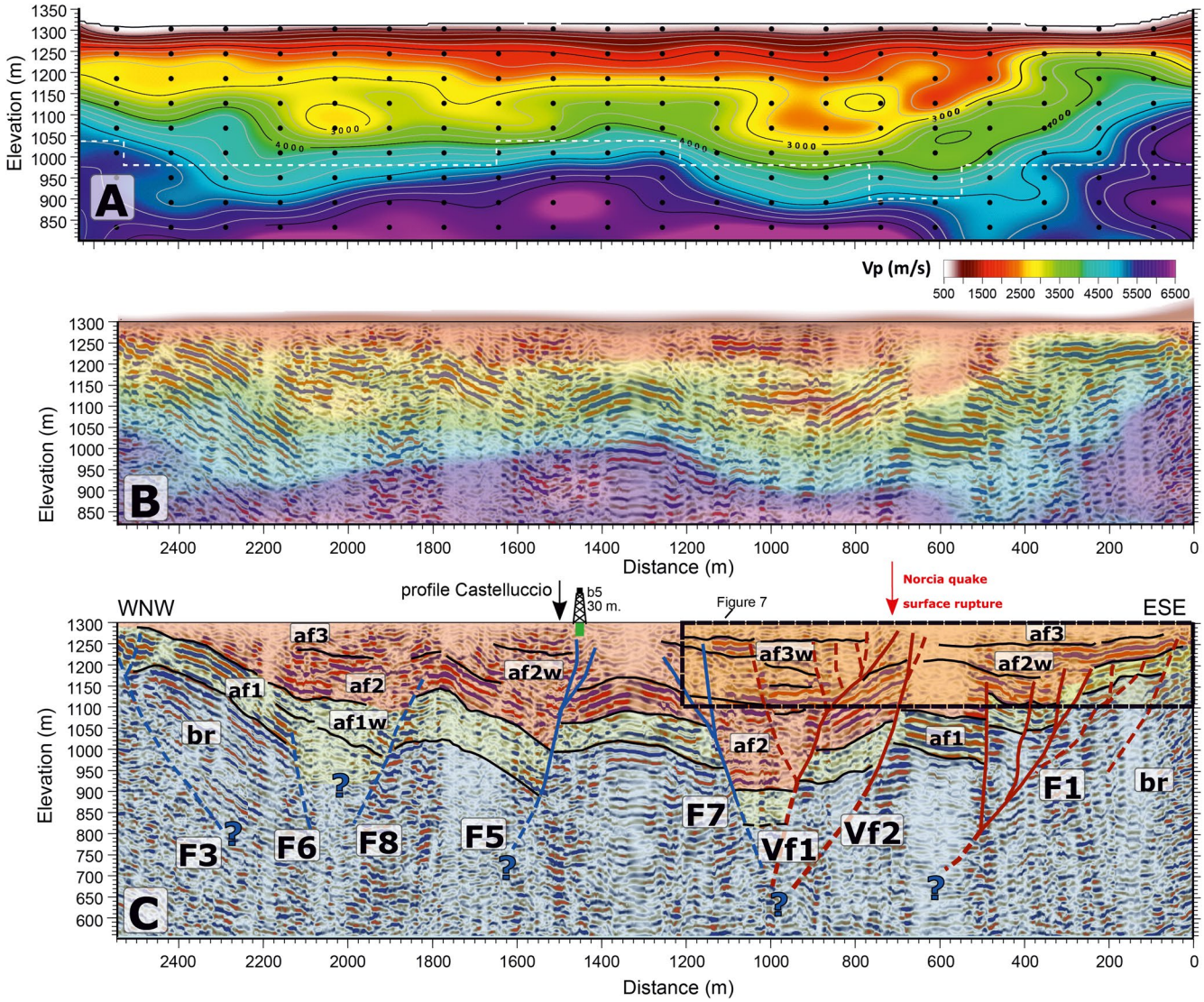

Figure 6. Results for Vettore Profile. (a) Best-fit tomographic model (black small circles indicate the velocity grid nodes that represent the 264 inverted model parameters; iso-velocity contour spacing 250 m/s; resolution depth from checkerboard test is shown as dashed white line). (b) Uninterpreted depth-converted migrated stack section with superimposed tomographic model. (c) Simplified geological interpretation. The thin black lines indicate the main boundaries of subsurface sedimentary sequences (alluvial fan units af1, af2 and af3; br = limestone bedrock). Red lines are inferred faults of the Vettore–Bove fault-system. Blue lines are inferred faults belonging to a different system. The black arrow marks the intersection with the Castelluccio Profile. The green rectangle indicates the projected position and depth extent of borehole b5. The black rectangle delimits the region shown in Figure 7.

Quaternary alluvial bodies through a geomorphological approach (Figures 2b and 3). New fieldwork was supplemented by the use of standard aerial photo interpretation (stereopairs of years 1954–1955 at nominal scale of 1:33,000 scale by the Istituto Geografico Militare Italiano; http://www.igmi.org). We also used digital elevation models (DEM) obtained from vector topographic maps (http://www.umbriageo.regione.umbria.it/pagina/distribuzione-carta-tecnica-regionale-vettoriale-1-000) and satellite images (Delorme et al., 2020). Due to the lack of absolute dating, we propose relative ages of the alluvial sediments based on morphology and inset relationships with other Quaternary deposits (Section 4.1). We discuss the possible age of subsurface deposits surveyed by seismic profiles in Section 5.1 (details in Text S3).

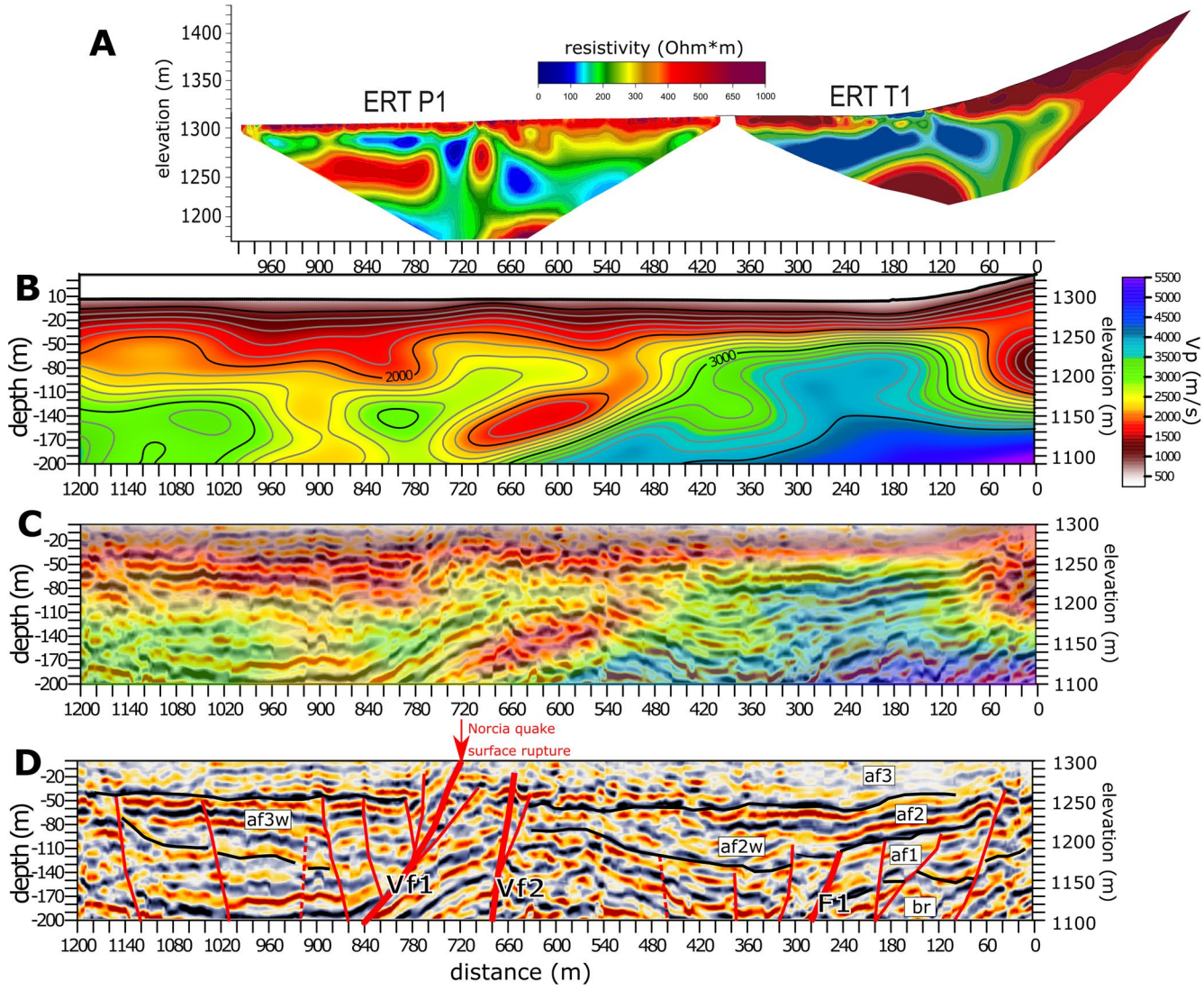

Figure 7. Detail of the shallow eastern portion of seismic profile Vettore, showing part of the fault zone ruptured during the 2016 M_W 6.5 mainshock. (a) Projected ERT profiles P1 (from: Villani & Sapia, 2017) and T1 (from: Villani et al., 2019). (b) High-resolution tomographic model obtained inverting 190 parameters (see details in Figure S7). (c) Zoom on the migrated and depth-converted section shown in Figure 6 with superimposed tomographic model after the application of automatic gain control (AGC; window of 0.1 s) to enhance weak reflections. (d) Interpretation of main faults (red lines) and stratigraphic boundaries (thin black lines). In this section, we report additional small-displacement faults barely visible in Figure 6c.

4. Results

Seismic imaging of fault-bounded continental basins filled with heterogeneous material is a challenging task. The seismic signal is usually contaminated by scattering and diffractions generated by coarse clastic deposits and by the irregular geometry of the subsurface interfaces (details in Text S2; Lawton, 1989; Stephenson et al., 2013). In addition, strong near-surface velocity variations make static corrections difficult. The presented migrated stack sections of the Castelluccio basin are of fair to good quality if we consider our challenging target dominated by coarse clastic infill. Some limitations are due to the poor lateral continuity of reflectors, and the presence of high-velocity breccia and conglomerates overlying the limestones, which often promote low-amplitude reflections from the substratum (Section 4.2). At places, zones of poor reflectivity are likely due to massive deposits. In such a complex setting, subsurface constraints provided by drilling are valuable for seismic interpretation. Unfortunately, the few shallow boreholes in the Castelluccio basin (Figure 3c) do not constrain the lithology of depositional sequences at depths >100 m. In addition, no absolute dating of subsurface sedimentary infill is available. Aware of these difficulties, we propose simple

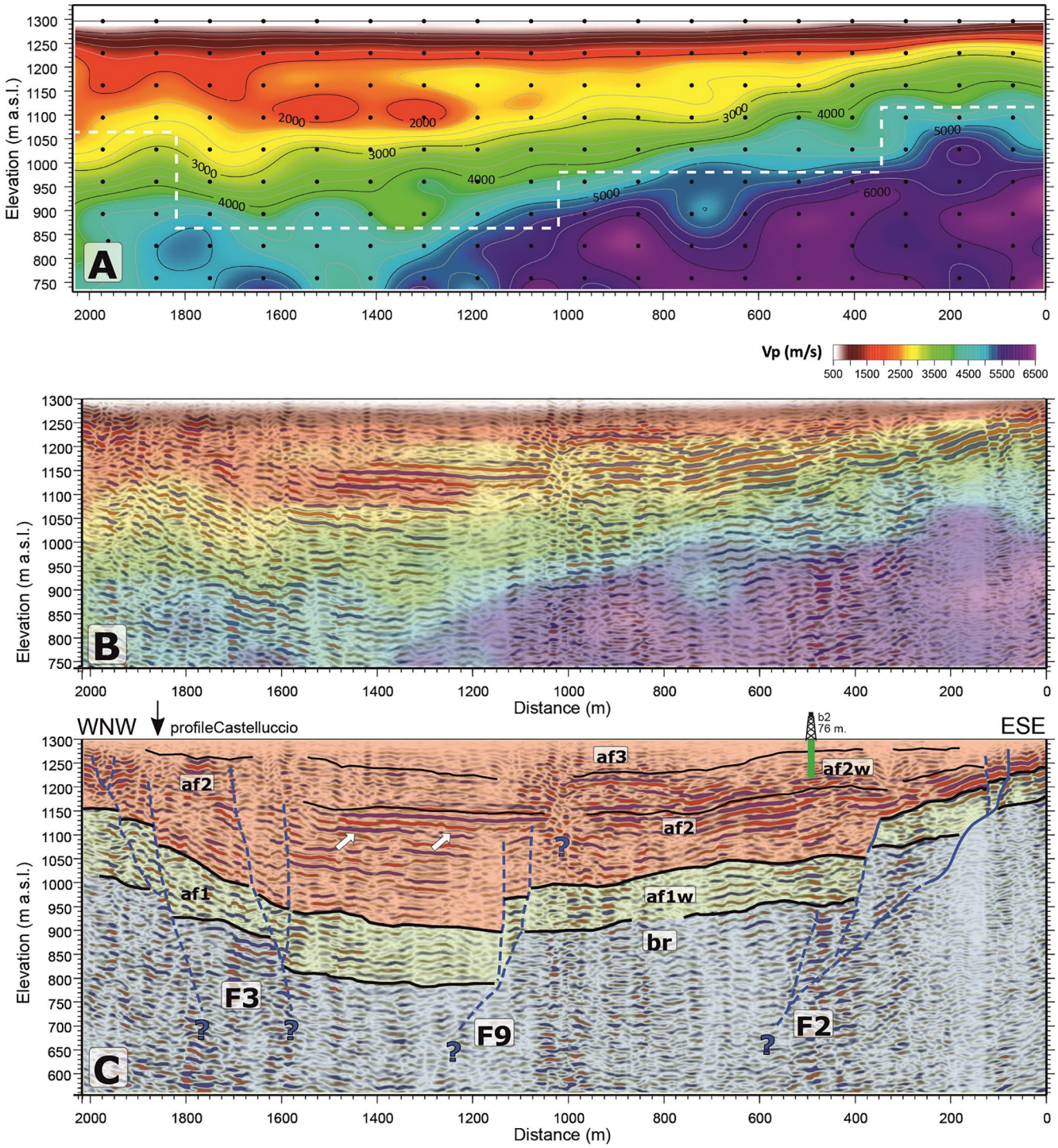

Figure 8. Results for Maneggio Profile. (a) Best-fit tomographic model (black small circles indicate the velocity grid nodes that represent the 180 inverted model parameters; iso-velocity contour spacing 250 m/s; white dashed line is resolution depth inferred from checkerboard test). (b) Uninterpreted depth-converted migrated stack section with superimposed tomographic model. (c) Simplified geological interpretation. The thin black lines indicate some of the main boundaries of subsurface sedimentary sequences (alluvial fan units af1, af2, and af3; br = limestone bedrock). Blue lines indicate inferred faults. Vertical black arrow shows the intersection with Castelluccio Profile. The small white arrows indicate low-Vp and well-stratified distal alluvial fan and palustrine deposits (see details in the text). The green rectangle indicates the projected position and depth extent of borehole b2.

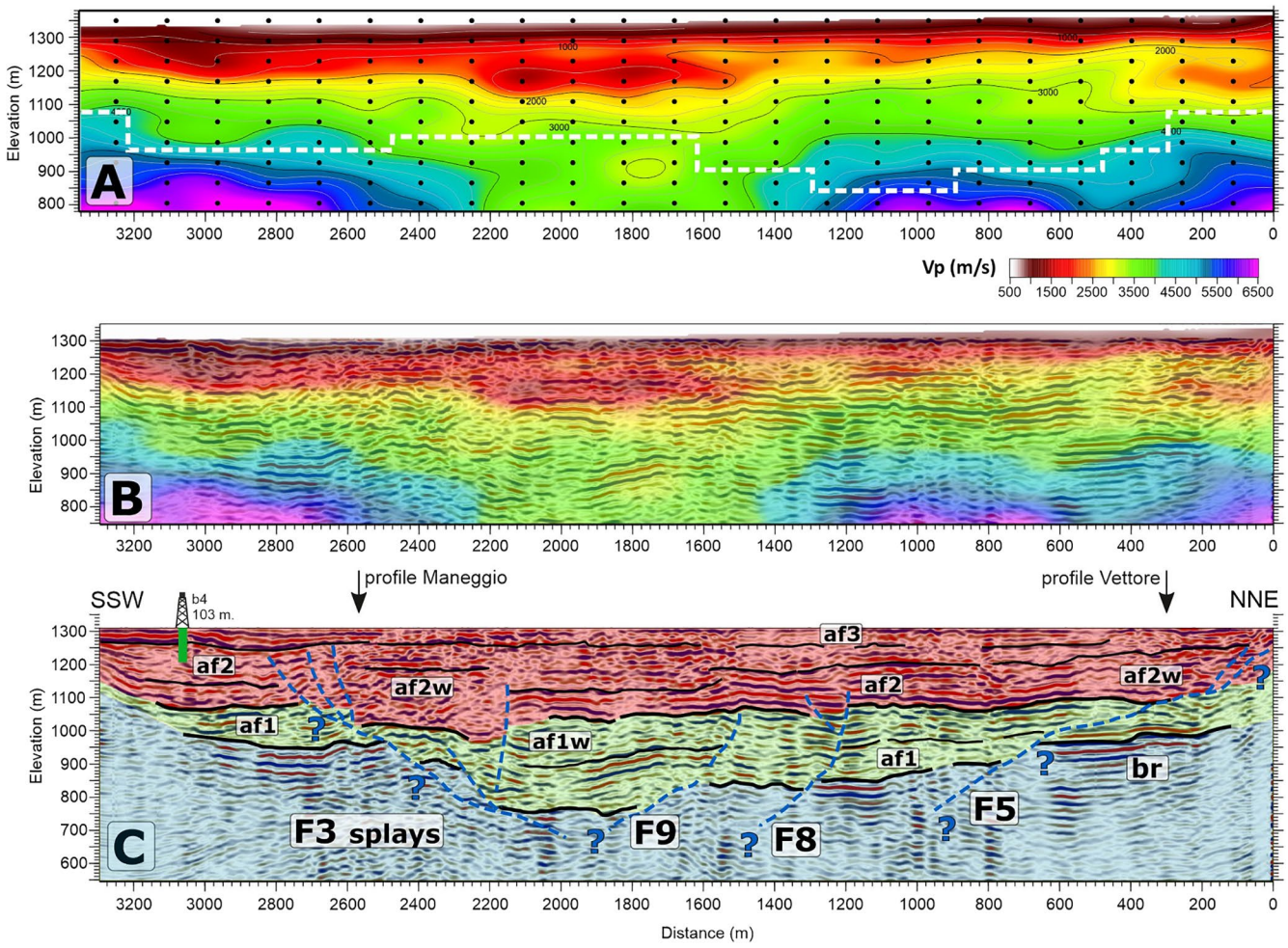

Figure 9. Results for Castelluccio Profile. (a) Best-fit tomographic model (black small circles indicate the velocity grid nodes that represent the 250 inverted model parameters; iso-velocity contour spacing 250 m/s). (b) Uninterpreted depth-converted migrated stack section with superimposed tomographic model. (c) Simplified geological interpretation. Thin black lines indicate the main boundaries of subsurface sedimentary sequences (alluvial fan units af1, af2, and af3; br = limestone bedrock). Blue lines are inferred faults. The green rectangle indicates the projected position and depth extent of borehole b2. Intersections with Vettore and Maneggio profiles are shown with vertical black arrows. The inferred faults F3 and F5 have an apparent low dip due to the orientation of the seismic profile.

tectonic and stratigraphic interpretations of the migrated stack sections (Sections 4.3–4.5). We highlight that they are not unique solutions and other interpretations are possible. In order to reduce the ambiguity, below we discuss the geological and geophysical constraints on stratigraphic interpretation, and on the estimation of the pre-Quaternary substratum location, as well as the resolution limits of seismic images.

4.1. Constraints on Seismic Stratigraphy

We have mapped several fan generations at the surface (Figures 2b and 3). The oldest ones form alluvial terraces to the north of the Castelluccio basin: they may be as old as the final part of Middle Pleistocene (e.g., Coltorti & Farabollini, 1995), since they are incised by outwash fans related to the Last Glacial Maximum (Galadini & Galli, 2003). The top surface of the distal fan lobes that grade into the present-day plain (4th alluvial generation in Figure 2b) ranges in age from Late Holocene to Recent (Galadini & Galli, 2003; Figure 3a).

The seismic profiles cross three large late Pleistocene–Holocene fans (Figure 3). In the northern part of the basin, the Valle delle Fonti fan displays a general southward progradation direction (darker lobes in Figure 3a). In the northern and central part of the Castelluccio basin, the >3 km-long and ~2 km-wide

Castelluccio fan has a gentle S-sloping surface that merges into a flat swampy area (Figures 2b and 3a). The Maneggio fan is >1,300 m-long, and it flows to the WNW from the flat-bottomed, ~80 m-wide and >100 m-deeply entrenched Bonanno Valley (Figures 2b and 3b).

In order to interpret subsurface lithology based on the *Vp* field, we use results of previous high-resolution refraction tomography surveys of intramontane basins in central and southern Apennines (Bruno et al., 2010, 2013; Improta et al., 2012; Morandi & Ceragioli, 2002; Villani, Pucci, et al., 2015, Villani, Tulliani, et al., 2015). Those studies document conglomerates and gravelly sands packages with *Vp* ~2,500–3,500 m/s, so we relate the tomographic *Vp* in the shallow part of our models to sandy gravels and subordinate silts. Based on reflection configuration, we infer the overall basin infill is composed of three main unconformity-bounded sequences of prevailing alluvial deposits, labeled as *af1*, *af2*, and *af3*, from bottom to top, respectively.

Unit *af1* has an average *Vp* > 3,000 m/s, and it generally shows poor organization, suggesting clastic deposits with rough stratification. Units *af2* and *af3* are characterized by a wide range of *Vp* (1,000–3,000 m/s), with lower values due to a lesser degree of compaction with respect to deeper deposits. These units are depicted by continuous and high-frequency reflections suggesting well-bedded alternating coarse and fine-grained deposits. We assume that unit *af3* includes the distal portions of the most recent generations of surface alluvial fans (final part of Middle Pleistocene to Holocene; Figure 2b). Conversely, it is difficult to correlate the deeper *af2* and *af1* units with any outcropping formation. Within units *af1*, *af2*, and *af3*, we also recognize some wedge-like packages associated with lateral *Vp* decrease (labeled as *af1w*, *af2w*, and *af3w*). They may be indicative of syn-tectonic deposition in the hanging wall of normal faults.

4.2. Resolution Limits of the Migrated Sections, and Strategy for Top-Bedrock and Fault Detection

Spatial resolution limits of the migrated stack sections depend on the dominant wavelength and the average velocity. From tomography, the shallowest 150 m layer has an average *Vp* of ~2,250 m/s and the first 0.1 s Two Way Time (TWT) of stack sections have a dominant frequency of ~50 Hz. For the deeper parts of tomographic models (800–1,150 m a.s.l.), the average *Vp* is ~4,700 m/s, and in the range 0.1–0.8 s TWT of the stack sections the dominant frequency is ~40 Hz. According to the quarter wavelength rule, those values imply a theoretical vertical separation limit of ~12 m in the shallow part and of ~30 m in the deeper part. These resolution restrictions provide a lower bound for the uncertainty in the location of the main reflectors interpreted as key markers.

Refraction tomography constrains the location of the pre-Quaternary limestone substratum (top-bedrock for short). At source-receiver distances >700–800 m, many common-shot gathers (CSGs) show first-arrivals that suggest high-velocity seismic interfaces (i.e., *Vp* > 4,500 m/s). Those interfaces appear as high-gradient belts with *Vp* ~4,500–5,000 m/s that we consider as a proxy for the top-bedrock. In fact, critically refracted waves at far offset traces are associated with first-arrival traveltime curves showing apparent *Vp* > 4,500 m/s (Figures 4 and 5).

A thin-bedded limestone bedrock should appear as strongly reflective. However, the occurrence of coarse and high-*Vp* clastic deposits unconformably overlying limestones hampers the generation of clear reflections useful to interpret the top-bedrock. Thus, we overlap the tomographic velocity field onto the migrated depth-converted sections. The spatial resolution of the tomographic models (Section 3.1) indicates that the nominal uncertainty in the estimation of the top-bedrock depth is ~60–80 m. Results from a recent 3D ERT survey performed in the area by Sapia et al., (2021) show that the high-resistive limestone substratum ($\rho \sim$ 700–1,000 **Ω**m) is in good agreement with the depth of high-*Vp* regions.

Concerning fault detection, we crosscheck lateral tomographic *Vp* changes and reflector truncations (Figures 6–9). The tomographic models display strong lateral *Vp* changes (locally >20%) producing steps and bumps in the top-bedrock, which represent smeared images of steeply dipping fault zones. We also recognize at places low-*Vp* round-shaped bodies characterized by a vertical velocity inversion (Figures 6a and 7b). Several tomographic surveys show that such low-*Vp* sags match poorly consolidated wedges and colluvial packages in the hanging wall block of active normal faults (e.g., Buddensiek et al., 2007; Mattson, 2004;

Morey & Schuster, 1999; Villani, Pucci, et al., 2015; Villani, Tulliani, et al., 2015; Villani et al., 2017; Villani, D'Amico, et al., 2018).

Fault dip is difficult to estimate. The reflection sections suggest the occurrence of high-angle faults (>60°) and prevailing normal displacements, in accordance with the local structural setting (Section 2). Due to the uncertain fault dip and the limitations of the 2-D sections, we can only infer the vertical component of slip (throw), and assume that oblique components are negligible. This assumption takes into account the dominant dip-slip coseismic kinematic indicators observed on the ruptured strands of the Vettore–Bove fault-system (Villani, Pucci, et al., 2018) and is consistent with long-term fault striae (e.g., Calamita, Pizzi & Roscioni, 1992). Vertical separation of displaced reflectors provides fault throw. Due to the aforementioned resolution limits, in principle our seismic images enable locating shallow faults with throws >15 m and deeper faults with throws >30 m.

4.3. Vettore Profile

This profile intercepts the 2016 coseismic surface ruptures along the VF fault at $x \sim 710$ m, and crosses the Valle delle Fonti and Castelluccio alluvial fans (Figure 3a).

The tomographic model shown in Figure 6a is on average resolved down to a depth of ~330–350 m, with a maximum resolution depth of ~400 m ($x = 550$–750 m; Figures S5 and S6). The model shows high-*Vp* zones (>4,000 m/s) at depths of ~100 m, ~350 and ~250 m in the western, central and eastern parts, respectively. Above the high-*Vp* zone, a ~100–150 m-thick region with *Vp* ~3,000 m/s thins eastwards, where it grades into a wide low-velocity area ($Vp < 2{,}500$ m/s). The shallowest low-*Vp* layer (<2,000 m/s) thickens around $x = 800$ m.

In the migrated depth-converted reflection section (Figure 6b), the adopted processing enhances the amplitude of energetic phases, in particular below 100 m depth, where high-amplitude and steep reflectors with variable dips are seen. The architecture of the low-amplitude shallow region at $x \sim 600$ m is clearly visible in the zoom in Figure 7c described in the following.

By using borehole *b5* (Figure 3c) and ERT profiles of Villani and Sapia (2017) and Villani et al. (2019) (Figure 7a), we interpret the very shallow reflectors as packages of alluvial sandy gravels. In the eastern part ($x = 300$–1,200 m), we relate unit *af2* to the basal portion of the Valle delle Fonti fan (Figure 6c). Moving to the west ($x = 700$–1,200 m), we relate unit *af3* to the basal part of the Castelluccio fan and to the most recent part of the Valle delle Fonti fan (Figure 3a). Units *af3* and *af2* are on average ~100–150 m and ~200–250 m-thick, respectively. They display local thickening to form wedges indicative of syn-tectonic deposition (units *af2w* and *af3w*; Figures 6c and 7d).

Units *af2* and *af3* lay over a ~100–150 m-thick alluvial unit (*af1*) characterized by poor reflectivity in the central part, possibly caused by lack of clear velocity contrasts and by coarser grain size. The deeper and high-amplitude reflections are associated with *Vp* ~2,500–3,000 m/s, and they likely represent well-bedded gravels and sands.

In the eastern part of the profile, a main W-throwing fault zone ~200 m-wide and composed of several smaller splays is visible at the base of Mt. Vettore (F1, at x ~120–300 m in Figure 6). This fault zone affects the limestone substratum with a total vertical displacement of ~150–250 m, evaluated from the height of the step in the high-*Vp* region and from the cumulative offset of the top-basement reflectors.

To better illustrate the shallow subsurface along this key sector of the profile, we complement the imaging with: (a) a higher resolution tomographic model, obtained using a finer parametrization (Figures 7b and S7); (b) a zoom on the migrated stack section after the application of an amplitude recovery tool (automatic gain control–AGC) that allows enhancing weak reflections (Figures 7c and 7d). Fault zone F1 affects the alluvial units *af1* and *af2*, promoting thickening of wedge unit *af2w* (Figure 7d). Although the eastern end of the seismic profile is characterized by low fold coverage (Figure S2) and by a shallower resolution depth of the tomography (Figure S7), we suggest the presence of a further splay at $x \sim 40$–60 m. Here, the upper fault tip is ~30 m-deep, consistent with the sub-vertical low-resistivity region in the co-located ERT profile T1 (at $x \sim 50$–60 m in Figure 7a).

In the hanging wall of fault F1, we detect two additional W-throwing subsurface faults: Vf2 at $x \sim 650$ m, and Vf1 at $x \sim 740$ m (Figures 6, 7b, 7c and 7d). Vf1 matches the VF fault, which ruptured the surface during the M_W 6.5 Norcia earthquake (Section 2; Figures 2 and 3a). Seismic evidence of fault Vf1 is outlined by a low-*Vp* shallow wedge located just in front of the Norcia earthquake scarp (Figure 7b). This wedge, defined by the abrupt westward deepening of the ~2,100 m/s velocity contour, is characterized by a ~30% drop in velocity with respect to the footwall block (*Vp* ~2,800–3,000 m/s; Figure 7b). This is paired with the sub-vertical and low-resistivity region ($\rho < 150$ Ωm) in the central part of the ERT profile P1 (Figure 7a). In the hanging wall of Vf1, dipping reflections show back-tilting of unit *af3w* toward the east. Unit *af3w* also shows hints of growth strata affected by small antithetic splays. Taken together, these features point to syn-tectonic deposition of *af3w*.

Fault Vf2 branches toward the surface, and it seems to affect the basal part of unit *af3*, with a minimum throw of ~30 m. This zone also displays a W-dipping low-*Vp* sag (<2,000 m/s at $x = 540$–720 m and ~150 m depth), consistent with the attitude of the reflectors. We interpret this zone as a silty-sandy package interlayered in the thick alluvial fan cover.

Possibly, a steep fault-zone dipping to the east bounds the western side of the basin (F3 at $x = 2{,}200$ m) coupled with an additional E-throwing fault at $x = 2{,}100$ m (see Figure 6c), which is in accordance with subsurface fault F6 (Figures 1c and 2a) previously hypothesized by Villani et al., (2019). In the central part of the profile, we also suggest subsidiary conjugate faults (F5, F7, and F8) that control the large-scale geometry of the substratum. The latter forms a horst-like structural high ($x = 1{,}100$–1,600 m) delineated by a high-*Vp* bump. This culmination may be the buried counterpart of the limestone hill to the north-west, where the village of Castelluccio di Norcia is located (Figure 2a). Fault F5 controls the sedimentation of alluvial unit *af2w*, and possibly affects the basal part of unit *af3* (Figure 6c).

4.4. Maneggio Profile

This profile crosses the Maneggio alluvial fan, and the eastern part is located in the Bonanno Valley ($x = 0$–250 m; Figure 3b).

The tomographic model (Figure 8a) is resolved down to a depth of ~250 m in the eastern part, ~350–400 m in the center and ~200 m in the western part (Figure S8). The top-bedrock (*Vp* > 4,500 m/s) slopes toward the western side of the basin down to ~350 m depth, and is >120 m-deep at the eastern end. The adjacent borehole *b2*, located closer to the right valley flank, reached shallower limestones (Figure 3c), suggesting that the seismic profile is likely parallel to a deep incision of the substratum. The shallow low-*Vp* (<2,500 m/s) reaches a thickness of ~200 m at $x = 1{,}200$ m. Within the basin infill, a low-*Vp* zone (*Vp* < 2,000 m/s) appears in the western-central sector ($x = 1{,}200$–1,600 m) at ~150–200 m depth.

The depth-converted migrated reflection section shows from the top to the bottom several alluvial units (Figure 8c). The shallow unit (*af3*) corresponds to the Maneggio fan (Figure 3b). Its maximum thickness is ~70–90 m at $x = 800$ m. Below this shallow unit, a well-bedded and ~200–250 m-thick package corresponds to unit *af2* thinning toward the east. In the deeper part, we recognize high-amplitude reflectors corresponding to a region of very high *Vp* (~4,500–5,000 m/s) in the tomogram (Figure 8b): we hypothesize that they represent stiff clastic deposits (Figure 8c).

In the central and western parts of the section, a region of poor reflectivity grades laterally and downward into high-amplitude, low-frequency and continuous reflectors, which have average low-*Vp* (<2,000 m/s; white arrows in Figure 8c). We interpret them as prevailing fine and well-bedded silty sands (see boreholes *b2* and *b4*, Figure 3c), which represent distal alluvial fans, possibly with subordinate palustrine intervals.

In the eastern part of the profile, two closely spaced W-throwing faults are interpreted as the subsurface structure of the border fault F2 (Figure 8c). The westernmost fault is outlined by a >100 m-high step in the top-bedrock at $x = 300$–500 m (Figure 8a) and displaces only the lower part of unit *af2*. Conversely, the eastern splay of fault F2 controls the deposition of unit *af2* and seems to displace also shallow layers (at least 30 m deep). Nevertheless, the vertical offset of the shallow units is very small (~10 m), and therefore close to the resolution limits of seismic data.

The westernmost part of the section is difficult to interpret, due to the lower fold coverage and shallower resolution of the tomographic model (Figures S3 and S8). A bump in the region with *Vp* ~3,000–4,000 m/s (x = 1,700–1,800 m) and reflector truncations suggest a couple of closely spaced E-throwing faults, which we tentatively interpret as splays of the basin-bounding fault F3 (Figure 2a).

In the middle of the seismic section, we infer the occurrence of a high-angle fault zone (F9 at x = 1,100–1,200 m), which downthrows the top-bedrock by ~100–150 m and affects units *af1* and *af2*. The depth of the top-bedrock in this part of the section (~450–500 m) is in agreement with 3D ERT data (Sapia et al., 2021).

4.5. Castelluccio Profile

The tomographic model in Figure 9a is resolved down to ~450 m b.g.l. in the northern part (Figure S9). The velocity field depicts in the northern and southern sides a gently dipping substratum, which deepens in the central part down to ~500 m depth, although this region is not well resolved. This finding is consistent with the low-frequency peak of the H/V curves (f_0 ~0.3–0.4 Hz) estimated in this part of the basin (Villani et al., 2019). Tomography also points out a ~100 m-thick and very low-*Vp* region (<2,000 m/s) located at x = 1,600–2,200 m, and delineated by a subtle velocity reversal at the top.

The depth-converted migrated stack section (Figure 9b) shows high-amplitude and continuous reflectors, indicating well-bedded deposits with lateral continuity: this proves that the profile is mostly parallel to the dominant flow direction of the main alluvial units. The wide extent of the shallow unit *af3* matches the surface extent of the Castelluccio fan (Figures 3b and 9c). Between 1,600 and 2,200 m and below *af3*, high-amplitude reflectors match the low-*Vp* zone (<2,000 m/s), interpreted as silts and of distal alluvial fan facies, similar to those recognized on the Maneggio Profile (Figure 8c). In the deeper part, the alluvial fan unit *af1* thickens at x = 1,600–2,200 m.

The orientation of the seismic profile (~N30° in the northern section and ~N50° in the central and southern parts) is nearly parallel to the border faults F2 and F3. Considering the obliquity of the Castelluccio profile with respect to Vettore and Maneggio profiles (~70° and ~80°, respectively), we would expect apparent dips of ~30° for fault F5 and ~25° for fault F3 at profile intersections. Some subtle reflection truncations, which suggest the occurrence of faults with an apparent low dip (~30°) consistent with the geometry of faults F3 and F5, support this interpretation.

We infer a couple of additional faults in the central part of the section (Figure 9c), and which may correspond to faults F8 and F9 recognized in the other two profiles (Sections 4.4 and 4.5).

5. Discussion

5.1. Shallow Architecture and Quaternary Activity of the Southern Portion of the Fault System Ruptured in the 2016 M_W 6.5 Earthquake

In the light of the results described in Section 4, here we discuss the shallow architecture of the southern portion of the Vettore–Bove fault system ruptured in 2016. Seismic profile Vettore provides the first high-resolution subsurface image of the western portion of a ~2 km-wide deformation zone, straddling the Cordone del Vettore and the VF faults, which accommodated a large fraction of surface slip of the M_W 6.5 mainshock (Section 2.1; e.g., Brozzetti et al., 2019; Delorme et al., 2020; Perouse et al., 2018; Pizzi et al., 2017; Villani, Pucci et al., 2018; Wilkinson et al., 2017). We discuss geometry, displacement and possible throw-rates of some subsurface faults that were partly unknown before this study, by describing a transect in the northern part of the Castelluccio basin (trace A–A′–A″ in Figure 2). The main results are summarized in the interpretative cross-section of Figure 10.

In the eastern part of the transect, the Cordone del Vettore fault and its synthetic splay DF produce long-term throw >400 m affecting the Mesozoic substratum (Figure 1c; e.g., Brozzetti et al., 2019). The short-term throw since the Last Glacial Maximum is > 20 m, implying Late Pleistocene throw-rates of ~0.8–1.0 mm/yr (e.g., Galli et al., 2019; Pucci et al., 2021; Puliti et al., 2020).

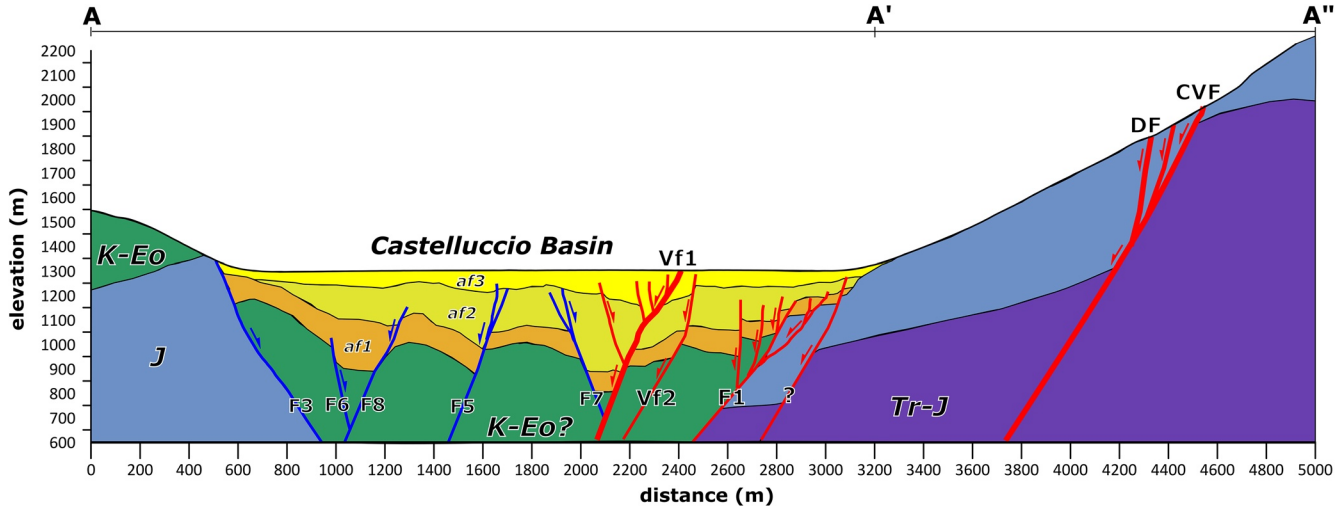

Figure 10. Interpretation of the shallow structure of the Castelluccio basin across the southern part of the Vettore–Bove fault system ruptured during the 2016 Norcia earthquake. The trace of section A–A′–A″ is reported in Figure 2a. For the meaning of fault labels and stratigraphic markers, refer to Figure 1c and the main text. Red lines with thicker stroke are splays of the Vettore–Bove fault system that ruptured the surface during the 2016 M_W 6.5 mainshock. Thin blue lines are faults belonging to a different system.

In the middle of the transect, for the VF fault Galadini and Galli (2003) inferred late Holocene throw-rates of 0.11–0.36 mm/yr, and Villani and Sapia (2017) proposed late Pleistocene throw-rates of ~0.2 mm/yr based on the ~5 m vertical displacement and cross-fault thickening of the Last Glacial Maximum fan (Section 2.1).

Crosscut relationships between deposits and faults would constrain the Quaternary evolution of the surveyed subsurface faults (Figure 10). Since no absolute dating of the deep alluvial infill is available (Section 2), we propose a hypothetical chronological scheme. We constrain this scheme based on: (a) long-term sedimentation rates of ~0.2–0.3 mm/yr (details in Text S3), (b) comparison with other fault-bounded basins in the central Apennines (e.g., Bosi et al., 2003; Cavinato et al., 2002; Civico et al., 2017; Cosentino et al., 2017; Giaccio et al., 2019; Giraudi et al., 2011; Macrì et al., 2016; Pucci et al., 2019). We thus suggest an age of ~0.6–0.4 Myr for the base of unit *af3*. Unit *af2* probably deposited between the Early and Middle Pleistocene (~0.6–1.7 Myr ago), while unit *af1* is likely Early Pleistocene in age (~2.3–1.7 Myr). Given these large uncertainties, we focus on the most recent evolution of the VF and F1 faults, which are better constrained by high-resolution seismic images and by surface geological data.

Seismic profile Vettore (Figures 6c and 7) shows that the subsurface of the VF fault consists of two splays, Vf1 and Vf2, which produce an aggregate throw of ~150–200 m. The thickness of the overall alluvial sequence *af1+af2+af3* is ~450 m in the hanging wall and ~300 m in the footwall of fault Vf1, suggesting syn-depositional faulting throughout the Quaternary. Recent fault activity is attested in the hanging wall by the wedge-shaped unit *af3w* (from growth and back-tilted strata), paired with a prominent low-*Vp* sag (<2,200 m/s; Figures 7b–7d). The cross-fault thickening of unit *af3* from ~50 to ~100–120 m implies a minimum vertical offset of ~50–70 m. Thus, our conservative estimate of throw-rate for fault Vf1 in the past ~0.5 Myr is ~0.1 mm/yr: this result suggests that the lower bound inferred from paleoseismic investigations is representative of the long-term throw-rate.

The splay Vf2 displaces the basal part of the alluvial fan unit *af3* by ~30 m, and its upper fault termination is very shallow (~10 m deep at least) denoting activity in the Late Pleistocene (Figure 7d).

Regarding fault F1, it consists of a ~200 m-wide fault zone comprising several splays (Figures 6c and 7). Overall, they control the sedimentation of unit *af2w*, and do not seem to affect unit *af3* except an inferred eastern splay (located at *x*~40–60 m in Figure 7c). ERT data indicate that this splay is covered by ~30–40 m-thick resistive alluvial deposits (Figure 7a), although Villani et al., (2019) do not rule out possible small recent displacements. We conclude that fault zone F1 was active up to the Middle-Late Pleistocene at least (Figure 10).

Whereas the total fault throw of fault zone F1 is ~1,200–1,400 m (e.g., Brozzetti et al., 2019; Calamita, Pizzi & Roscioni, 1992; Villani et al., 2019; Figures 1c and 10), the amount of Quaternary displacement is a matter of debate (e.g., Bonini et al., 2019; Buttinelli et al., 2021). Porreca et al., (2020) suggest that all the fault displacement accrued during the Quaternary. Pizzi and Scisciani (2000) infer a Quaternary throw of ~800 m, by using the vertical offset of upland planation surfaces carved on the Meso-Cenozoic substratum. Our seismic data (Figure 6c) indicate that fault zone F1 downthrows the top-bedrock by ~150–250 m. Therefore, the Quaternary throw of the compound fault zone F1+Vf1+Vf2 is ~400 ± 100 m (Figures 6c and 10). Such a value would represent a minimum estimate of the total Quaternary displacement, because the stratigraphic record in the hanging wall may be incomplete, due to partial removal of sediments in the very early stage of basin formation. However, considering the maximum thickness of the continental infill (~500 m) and the negligible incision of the Late Pleistocene to Recent top alluvial surface, our seismic data (Figures 6 and 7) suggest that part of the large geologic throw of the border fault zone F1 predates the formation of the Castelluccio basin. Subsequently, due to growth of the Vettore–Bove fault-system, fault F1 was involved in the development of the northern part of this depression.

We summarize our main results as follows. The westernmost part of the coseismic deformation zone of the 2016 M_W 6.5 earthquake comprises several subsurface faults, including F1, Vf1, and Vf2. We interpret Vf1, Vf2 and the associated subsidiary faults as splays of the major border fault F1, from which they likely branch off (e.g., McGrath & Davison, 1995). This is consistent with published seismotectonic models, where the deep M_W 6.5 mainshock fault branches at the surface into several sub-parallel SW-dipping splays (e.g., Brozzetti et al., 2019; Villani et al., 2019). Fault Vf1 has been active since the Middle Pleistocene, with long-term throw rates of ~0.1 mm/yr. Hanging wall seismic stratigraphy shows that Vf1, during sedimentation of unit *af3*, accommodated a large part of deformation of the ~1 km-wide fault zone bordering to the east the Castelluccio basin. Fault Vf2 displaces the base of unit *af3* by ~30 m and was active up to the Late Pleistocene at least. Fault F1 has a minimum Quaternary throw of ~150–250 m. The aggregate throw of the fault zone F1+Vf1+Vf2 is ~400 ± 100 m, suggesting that part of the total vertical displacement affecting the Meso-Cenozoic units (~1,200–1,400 m; Brozzetti et al., 2019; Calamita, Pizzi & Roscioni, 1992; Villani et al., 2019) likely pre-dates the Castelluccio basin.

5.2. Structure and Evolution of the Castelluccio Basin

The investigation depth of ~500–600 m achieved by our seismic profiles enables a reconstruction of the Quaternary evolution of the Castelluccio basin and its bounding faults. Due to the uncertain chronology of the subsurface deposits (Section 5.1), here we summarize a few main points and working hypotheses.

Our seismic images provide evidence of a dominant extensional origin of the Castelluccio basin. The latter results from the interplay of non-collinear normal faults during the Quaternary.

While surface faults F1 and VF trend NNW-SSE, a NE-SW strike of buried faults F2, F3, and F9 is inferred from their steep attitude as seen in the Maneggio Profile (Figure 8c). This trend is also suggested by a recent 3D ERT survey (Sapia et al., 2021), by the geomorphology of the mountain fronts bordering the basin and by the preferential direction of fast shear waves from local micro-earthquakes (Villani et al., 2019; Figures 1c and 2a).

Concerning the Quaternary activity of the faults trending N20°–40°, we infer that faults F2, F3 and subordinately F9 (Figure 8c) created the accommodation space filled by the oldest alluvial fan units *af1* and *af2*. Fault F2 controlled the deposition of the sequences *af1* and *af2w*, whereas possible metrical displacements affecting unit *af3* are close to the resolution limit of seismic data (<10 m). We thus suggest a low degree of activity for fault F2 since the Late Pleistocene. In fact, there is no clear morphotectonic indication of a recent fault scarp on the Maneggio fan at the mountain front intersection (Figure 3b). Moreover, this fan displays some morphometric features, such as a large *sweep* angle coupled with gentle slope of the top surface, and low amount of channel incision (Figure 3b), which are indicative of a low rate of fault-controlled local base-level fall (e.g., Villani & Pierdominici, 2010; Viseras et al., 2003; Whipple & Trayler, 1996). Fault F9 partly controlled the deposition of unit *af1*, and its activity ceased during the deposition of unit *af2*. As regards the faults interpreted as synthetic splays of F3, they affect unit *af2* and do not offset unit *af3*.

On the other hand, the NNW-trending faults in the northern part of the basin are active (Vf1 and possibly Vf2) or ceased activity in the late Pleistocene (F1).

Summarizing, the genesis of the Castelluccio basin was controlled by coeval activity of faults trending N20°–40° (F2, F3, and F9), and N150°–170° (F1), presumably since the Early Pleistocene. During this time interval, other intra-basin faults with different orientation were active (e.g., F5, F8). Later on, likely since the Middle Pleistocene, deformation was mostly accommodated by the NNW-trending fault zone including F1, Vf2, and Vf1. This latter fault also ruptured during the 2016 M_W 6.5 mainshock.

5.3. Relations Between the Vettore–Bove Fault System and Transverse Faults

Different mechanisms can generate non-collinear normal fault systems, including multi-phase extension, local stress perturbations and reactivation of pre-existing faults (Henza et al., 2010, 2011; Maerten et al., 2002; Morley, 2010, 2016; Reeve et al., 2015; Scisciani et al., 2018, 2019). Possibly, the Castelluccio basin results from a combination of a single NE-directed extensional phase (current SH_{max} trending N140°–150°; Montone & Mariucci, 2016; Figure 1b), with the involvement of pre-Quaternary and neo-formed normal faults.

The relationships between the transverse faults trending N20°–40° (in particular F2, F3, F8, and F9) and the NNW-trending Vettore–Bove fault-system are not clear. Probably, the transverse faults derive from previous tectonic phases (e.g., Buttinelli et al., 2021; Calamita, Pizzi & Roscioni, 1992; Calamita et al., 2012; Pierantoni et al., 2013). Alternatively, they may have developed as secondary structures due to local stress-reorientation close to the southern segments of the Vettore–Bove fault-system (e.g., Maerten et al., 2002). Numerical modeling of stepping normal faults indicate that transverse faults may develop although oblique to the dominant extension direction (Hodge et al., 2018).

Given this complex setting, we do not definitively rule out current activity of NE-trending faults in the study area. Indeed, the rupture of a deep ~N200°-trending subsidiary fault underneath the Castelluccio basin during the M_W 6.5 mainshock has been proposed by Scognamiglio et al., (2018) and Walters et al., (2018), based on inversion of strong motion and geodetic data.

Moreover, the high-quality aftershocks catalog of the 2016 sequence documents that NNE-trending faults can slip with normal kinematics even if they are not optimally oriented within the present-day stress field (Improta et al., 2019).

Our reconstruction of the Castelluccio basin evolution suggests that long-term strain accumulation on major NW-trending normal faults in the Apennines may display local complexities, particularly due to the occurrence of transverse structures. Several studies indicate that this is a common feature of many Quaternary extensional basins in the Apennines (e.g., Bruno et al., 2013; Cavinato et al., 2002; Civico et al., 2017; Colella et al., 2004; Delle Donne et al., 2007; Galli et al., 2017; Patruno & Scisciani, 2021; Pucci et al., 2019).

6. Conclusions

In this study, we show three high-resolution seismic profiles acquired in the hanging wall of the southern portion of the Vettore–Bove fault-system, causative fault of the 2016 M_w 6.5 Norcia earthquake. We integrate refraction tomography and reflection data to obtain high-resolution, complementary *Vp* models and migrated stack sections. They provide details on the shallow fault architecture, as well as the structural setting of the Castelluccio hanging wall basin down to ~500–600 m depth.

The investigated part of the Vettore–Bove fault-system displays three main SW-throwing faults (labeled as F1, Vf1, and Vf2) spreading over a ~800 m-wide zone and including subsidiary smaller faults that were unknown before this study (Figure 10). We interpret Vf1, Vf2 and the associated subsidiary faults as splays of the major border fault F1. Faults F1, Vf2, and Vf1 display prominent growth strata in the hanging wall, attesting syn-tectonic deposition. Fault Vf1 is currently active and ruptured the surface during the M_w 6.5 mainshock. Cross-fault thickening of alluvial unit *af3* suggests a minimum vertical offset of ~50–70 m for which we infer a long-term throw rate of ~0.1 mm/yr in the past 0.5 Myr for Vf1. Fault Vf2 also affects the basal part of alluvial unit *af3*, suggesting activity up to the late Pleistocene.

Our results indicate that the minimum aggregate Quaternary throw of faults F1+Vf1+Vf2 is ~400 ± 100 m. We thus suggest that, for the major border fault zone F1, part of the large total throw affecting the Mesozoic units (~1,200–1,400 m) likely pre-dates the Castelluccio basin. During the Quaternary, this fault concurred to the development of the northern part of the depression, and probably ceased activity in the late Pleistocene.

Concerning the Castelluccio basin structure, seismic data indicate that its infill comprises alluvial sequences with a maximum thickness of ~500 m in the southern depocenter. As a working hypothesis, we infer that the Castelluccio basin results from the interplay of normal faults trending N20°–40° and N150°–170°. The relationships between the transverse faults trending N20°–40° and the NNW-trending Vettore–Bove fault-system are not clear. Probably, the transverse faults derive from previous tectonic phases, or they may have developed as secondary structures due to local stress-reorientation. Although oblique to the dominant extension direction, these transverse faults accommodated a portion of the deformation mostly hosted on the adjacent NNW-trending strands. By analogy with other deep Quaternary continental basins in the Apennines (e.g., Fucino basin: Cavinato et al., 2002; Patruno & Scisciani, 2021; Middle Aterno Valley: Cosentino et al., 2017; Pucci et al., 2019), the large thickness of the surveyed sedimentary infill suggests that the bounding faults likely activated in the Early Pleistocene. Since the Middle Pleistocene, displacement accumulation mostly affected the NNW-trending strands of the Vettore–Bove fault-system, including the activation of the VF fault.

As a more general remark, this work shows that combining high-resolution refraction tomography and reflection profiling, integrated with detailed field mapping, enables us to solve the architecture of a composite Quaternary normal fault network, and also to provide details on near-surface, active fault zones. This approach is solid and is suitable for application in similar active tectonic settings worldwide.

Data Availability Statement

Processing of refraction data has been performed with the Seismic Unix package (Cohen & Stockwell, 1995). Processing of seismic reflection data has been performed using SeisSpace® ProMAX® 2D software (https://www.landmark.solutions/SeisSpace-ProMAX). Figures have been prepared using the following software: Generic Mapping Tool (Wessel & Smith, 1998), Inkscape (https://www.inkscape.org), ArcMap (http://www.esri.com), Paraview v.5.8 (http://www.paraview.org) and Golden Software Surfer (http://www.goldensoftware.com/). Data supporting the conclusions can be found in the cited references, in the Supporting Information and in the repository available at the following link: https://doi.org/10.6084/m9.figshare.13469469.

Acknowledgments
This work has been funded by the Italian Civil Protection Department (DPC) under an agreement between Istituto Nazionale di Geofisica e Vulcanologia (INGV) and Centro di Geotecnologie (CGT) of Siena University, and by INGV Project Pianeta Dinamico (code C.U.P. D53J19000170001) financed by Ministry of Education, Universities and Research (MIUR) ("Fondo finalizzato al rilancio degli investimenti delle amministrazioni centrali dello Stato e allo sviluppo del Paese", legge n. 145/2018)-Task S2-2021. The views and conclusions contained in this paper are those of the Authors, and they should not be interpreted as necessarily representing official policies, either expressed or implied, of the DPC. We warmly thank: prof. Paolo Conti for fruitful collaboration during the planning stage of the seismic experiment; Valentina Cicala, Lisa Afeltra, Nico D'Intino, Marco Di Camillo, Simone Febo and Matteo Calorio for precious help during field work; Dr. Carlo Bifulco (president of the Mt. Sibillini National Park), Nicola Alemanno (mayor of Norcia), and the Carabinieri Forestali of Visso for providing the authorizations to perform the seismic experiment in the Pian Grande di Castelluccio basin; Roberto Pasqua (chair of Comunanza Agraria di Castelluccio) and the Provincial Police headquarters in Norcia (Uffici Comprensoriali Valnerina) for logistical support; Fausto Monti for hospitality in Montegallo village on September and October 2017. We acknowledge support of this work via a Landmark Grant Program to INGV, to the University of Siena and to the University of Naples Federico II by Halliburton Software and Services, a Halliburton Company, and dGB Earth Science academic license agreement for OpendTect Pro® software to the University of Siena.
An early version of the manuscript benefited from comments by Isabelle Manighetti and William J. Stephenson. We thank the Editor Taylor Schildgen and the Associate Editor Luca Dal Zilio for handling the new version of the manuscript. In particular, we kindly acknowledge Théa Ragon for her thoughtful comments and suggestions that helped us improve the overall quality of the paper. Open Access Funding provided by Istituto Nazionale di Geofisica e Vulcanologia within the CRUI-CARE Agreement.

References

Benedetti, L., Manighetti, I., Gaudemer, Y., Finkel, R., Malavieille, J., Pou, K., et al. (2013). Earthquake synchrony and clustering on Fucino faults (Central Italy) as revealed from in situ 36Cl exposure dating. *Journal of Geophysical Research: Solid Earth*, *118*, 4948–4974. https://doi.org/10.1002/jgrb.50299

Bigi, S., Conti, A., Casero, P., Ruggiero, L., Recanati, R., & Lipparini, L. (2013). Geological model of the central Periadriatic basin (Apennines, Italy). *Marine and Petroleum Geology*, *42*, 107–121. https://doi.org/10.1016/j.marpetgeo.2012.07.005

Blumetti, A. M., & Guerrieri, L. (2007). Fault-generated mountain fronts and the identification of fault segments: Implications for seismic hazard assessment. *Bollettino Società Geologica Italiana*, *126*, 307–322.

Boncio, P., Lavecchia, G., & Pace, B. (2004). Defining a model of 3D seismogenic sources for Seismic Hazard assessment applications: The case of central Apennines (Italy). *Journal of Seismology*, *8*, 408–425. https://doi.org/10.1023/b:jose.0000038449.78801.05

Bonini, L., Basili, R., Burrato, P., Cannelli, V., Fracassi, U., Maesano, F. E., et al. (2019). Testing different tectonic models for the source of the Mw 6.5, 30 October 2016, Norcia earthquake (central Italy): A youthful normal fault, or negative inversion of an old thrust? *Tectonics*, *38*, 990–1017. https://doi.org/10.1029/2018TC005185

Bosi, C., Galadini, F., Giaccio, B., Messina, P., & Sposato, A. (2003). Plio-Quaternary continental deposits in the Latium-Abruzzi Apennines: The correlation of geological events across different intermontane basins. *Il Quaternario, Italian Journal of Quaternary Sciences*, *16*(1bis), 55–76.

Brocher, T. M., Carr, M. D., Fox, K. F., & Hart, P. E. (1993). Seismic reflection profiling across Tertiary extensional structures in the eastern Amargosa Desert, southern NV, Basin and Range province. *The Geological Society of America Bulletin*, *105*(1), 30–46. https://doi.org/10.1130/0016-7606(1993)105%3C0030:SRPATE%3E2.3.CO;2

Brozzetti, F., Boncio, P., Cirillo, D., Ferrarini, F., De Nardis, R., Testa, A., et al. (2019). High resolution field mapping and analysis of the August–October 2016 coseismic surface faulting (Central Italy Earthquakes): Slip distribution, parameterization and comparison with global earthquakes. *Tectonics*, *38*(2), 417–439. https://doi.org/10.1029/2018TC005305

Bruno, P. P. G., Berti, C., & Pazzaglia, F. J. (2019). Accommodation, slip inversion and segmentation in a province-scale shear zone from high-resolution, densely spaced, wide-aperture seismic profiling, Centennial Valley, MT, USA. *Scientific Reports*, *9*, 9214. https://doi.org/10.1038/s41598-019-45497-1

Bruno, P. P. G., Castiello, A., Villani, F., & Improta, L. (2013). High-resolution densely spaced wide-aperture seismic profiling as a tool to aid seismic hazard assessment of fault-bounded intramontane basins: Application to Vallo di Diano, Southern Italy. *Bulletin of the Seismological Society of America*, *103*(3), 1969–1980. https://doi.org/10.1785/0120120071

Bruno, P. P. G., DuRoss, C. B., & Kokkalas, S. (2017). High-resolution seismic profiling reveals faulting associated with the 1934 Ms 6.6 Hansel Valley earthquake (Utah, USA). *The Geological Society of America Bulletin*, *129*, 1227–1240. https://doi.org/10.1130/B31516.1

Bruno, P. P. G., Improta, L., Castiello, A., Villani, F., & Montone, P. (2010). The Vallo di Diano Fault System: New evidence for an active range-bounding fault in southern Italy using shallow, high-resolution seismic profiling. *Bulletin of the Seismological Society of America, Short Notes*, *100*(2), 882–890. https://doi.org/10.1785/0120090210

Bruno, P. P. G., Maraio, S., & Festa, G. (2017). The shallow structure of Solfatara Volcano, Italy, revealed by dense, wide-aperture seismic profiling. *Scientific Reports*, *7*(1), 17386. https://doi.org/10.1038/s41598-017-17589-3

Buddensiek, M. L., Sheng, J., Crosby, T., Shuster, G. T., Bruhn, R. L., & He, R. (2007). Colluvial wedge imaging using traveltime and waveform tomography along the Wasatch Fault near Mapleton, Utah. *Geophysical Journal International*, *172*(2), 686–697. https://doi.org/10.1111/j.1365-246X.2007.03667.x

Bull, W. B. (2009). *Tectonically active landscapes*. Wiley. https://doi.org/10.1002/9781444312003

Burbank, D. W., & Anderson, R. S. (2011). *Tectonic geomorphology* (2nd ed.). Wiley-Blackwell. https://doi.org/10.1002/9781444345063

Buttinelli, M., Petracchini, L., Maesano, F. E., D'Ambrogi, C., Scrocca, D., Marino, M., et al., (2021). The impact of structural complexity, fault segmentation and reactivation on seismotectonics: Constraints from the upper crust of the 2016-2017 central Italy seismic sequence area. *Tectonophysics*, *810*, 228861. https://doi.org/10.1016/j.tecto.2021.228861

Calamita, F., Coltorti, M., Piccinini, D., Pierantoni, P. P., Pizzi, A., Ripepe, M., et al. (2000). Quaternary faults and seismicity in the Umbro-Marchean Apennines (Central Italy): Evidence from the 1997 Colfiorito earthquake. *Journal of Geodynamics*, *29*(3–5), 245–264. https://doi.org/10.1016/S0264-3707(99)00054-X

Calamita, F., Esestime, P., Paltrinieri, W., Scisciani, V., & Tavarnelli, E. (2009). Structural inheritance of pre- and syn-orogenic normal faults on the arcuate geometry of Pliocene-Quaternary thrusts: Examples from the central and southern Apennine Chain. *Italian Journal of Geosciences*, *128*(2), 381–394. https://doi.org/10.3301/IJG.2009.128.2.381

Calamita, F., Pace, P., & Satolli, S. (2012). Coexistence of fault-propagation and fault-bend folding in curve-shaped foreland fold-and-thrust belts: Examples from the Northern Apennines (Italy). *Terra Nova*, *24*(5), 396–406. https://doi.org/10.1111/j.1365-3121.2012.01079.x

Calamita, F., & Pizzi, A. (1992). Tettonica quaternaria nella dorsale appenninica umbro-marchigiana e bacini intrappenninici associati. *Studi Geologici Camerti*, *1*, 17–25. https://doi.org/10.15165/studgeocam-1186

Calamita, F., & Pizzi, A. (1994). Recent and active extensional tectonics in the southern Umbro-Marchean Apennines (central Italy). *Memorie Società Geologica Italiana*, *48*, 541–548.

Calamita, F., Pizzi, A., & Roscioni, M. (1992). I fasci di faglie recenti ed attive di M. Vettore – M. Bove e di M. Castello – M. Cardosa (appennino Umbro-Marchigiano). *Studi Geologici Camerti*, *1*, 81–95. https://doi.org/10.15165/studgeocam-1198

Carminati, E., Bignami, C., Doglioni, C., & Smeraglia, L. (2020). Lithological control on multiple surface ruptures during the 2016–2017 Amatrice-Norcia seismic sequence. *Journal of Geodynamics*, *134*, 101676. https://doi.org/10.1016/j.jog.2019.101676

Carminati, E., Lustrino, M., & Doglioni, C. (2012). Geodynamic evolution of the central and western Mediterranean: Tectonics vs. igneous petrology constraints. *Tectonophysics*, *579*, 173–192. https://doi.org/10.1016/j.tecto.2012.01.026

Catchings, R. D., Gandhok, G., Goldman, M. R., Okaya, D., Rymer, M.-J., & Bawden, G. W. (2008). Near-surface location, geometry and velocity of the Santa Monica fault zone, Los Angeles. *Bulletin of the Seismological Society of America*, *98*, 124–138. https://doi.org/10.1785/0120020231

Cavinato, G. P., Carusi, C., Dall'Asta, M., Miccadei, E., & Piacentini, T. (2002). Sedimentary and tectonic evolution of Plio-Pleistocene alluvial and lacustrine deposits of Fucino Basin (central Italy). *Sedimentary Geology*, *148*(1), 29–59. https://doi.org/10.1016/S0037-0738(01)00209-3

Chiaraluce, L., Di Stefano, R., Tinti, E., Scognamiglio, L., Michele, M., Casarotti, E., et al. (2017). The 2016 Central Italy seismic sequence: A first look at the mainshocks, aftershocks and source models. *Seismological Research Letters*, *88*(3), 757–771. https://doi.org/10.1785/0220160221

Cinti, F. R., De Martini, P. M., Pantosti, D. P. M., Baize, S., Smedile, A., Villani, F., et al. (2019). A 22-kyr-long record of surface faulting along the source of the 30 October 2016 earthquake (central Apennines, Italy), from integrated paleoseismic datasets. *Journal of Geophysical Research: Solid Earth*, *124*(8), 9021–9048. https://doi.org/10.1029/2019JB017757

Cirillo, D. (2020). Digital field mapping and drone-aided survey for structural geological data collection and seismic hazard assessment: Case of the 2016 central Italy earthquakes. *Applied Sciences*, *10*(15), 5233. https://doi.org/10.3390/app10155233

Civico, R., Pucci, S., Villani, F., Pizzimenti, L., De Martini, P. M., Nappi, R., & The Open EMERGEO Working Group. (2018). Surface ruptures following the 30 October 2016 Mw 6.5 Norcia earthquake, central Italy. *Journal of Maps*, *14*(2), 151–160. https://doi.org/10.1080/17445647.2018.1441756

Civico, R., Sapia, V., Di Giulio, G., Villani, F., Pucci, S., Baccheschi, P., et al. (2017). Geometry and evolution of a fault-controlled Quaternary basin by means of TDEM and single-station ambient vibration surveys: The example of the 2009 L'Aquila earthquake area. *Journal of Geophysical Research: Solid Earth*, *122*(3), 2236–2259. https://doi.org/10.1002/2016JB013451

Cohen, J. K., & Stockwell, J. W. (1995). SU user's manual. In Theory of seismic imaging. lecture notes in Earth sciences (Vol. 55, pp. 21–258). Springer. https://doi.org/10.1007/BFb0012094

Colella, A., Lapenna, V., & Rizzo, E. (2004). High-resolution imaging of the High Agri Valley Basin (Southern Italy) with electrical resistivity tomography. *Tectonophysics*, *386*(1–2), 29–40. https://doi.org/10.1016/j.tecto.2004.03.017

Coltorti, M., & Farabollini, P. (1995). Quaternary evolution of the Castelluccio di Norcia Basin. *Il Quaternario, Italian Journal of Quaternary Sciences*, *8*, 149–166.

Cosentino, D., Asti, R., Nocentini, M., Gliozzi, E., Kotsakis, T., Mattei, M., et al. (2017). New insights into the onset and evolution of the central Apennine extensional intermontane basins based on the tectonically active L'Aquila Basin (central Italy). *The Geological Society of America Bulletin*, *129* (9–10), 1314–1336, https://doi.org/10.1130/B31679.1

Cowie, P., Phillips, R. J., Roberts, G. P., McCaffrey, K., Zijerveld, L. J. J., Gregory, L. C., et al. (2017). Orogen-scale uplift in the central Italian Apennines drives episodic behaviour of earthquake faults. *Scientific Reports*, *7*, 44858. https://doi.org/10.1038/srep44858

Cowie, P. A., & Roberts, G. P. (2001). Constraining slip rates and spacings for active normal faults. *Journal of Structural Geology*, *23*, 1901–1915. https://doi.org/10.1016/S0191-8141(01)00036-0

D'Agostino, N., Avallone, A., Cheloni, D., D'Anastasio, E., Mantenuto, S., & Selvaggi, G. (2008). Active tectonics of the Adriatic region form GPS and earthquake slip vectors. *Journal of Geophysical Research*, *113*, B12413. https://doi.org/10.1029/2008JB005860

D'Agostino, N., Jackson, J. A., Dramis, F., & Funiciello, R. (2001). Interactions between mantle upwelling, drainage evolution and active normal faulting: An example from the central Apennines (Italy). *Geophysical Journal International*, *147*(2), 475–497. https://doi.org/10.1046/j.1365-246X.2001.00539.x

D'Agostino, N., Mantenuto, S., D'Anastasio, E., Giuliani, R., Mattone, M., Calcaterra, S., et al. (2011). Evidence for localized active extension in the central Apennines (Italy) from global positioning system observations. *Geology*, *39*, 291–294. https://doi.org/10.1130/G31796.1

Delle Donne, D., Piccardi, L., Odum, J. K., Stephenson, W. J., & Williams, R. A. (2007). High-resolution shallow reflection seismic image and surface evidence of the Upper Tiber Basin active faults (Northern Apennines, Italy). *Bollettino della Societa Geologica Italiana*, *126*(2), 323–331.

Delorme, A., Grandi, R., Klinger, Y., Pierrot Deseilligny, M., Feuillet, N., Jacques, E., et al. (2020). Complex deformation at shallow depth during the 30 October 2016 Mw6. 5 Norcia earthquake: Interference between tectonic and gravity processes? *Tectonics*, *39*(2). https://doi.org/10.1029/2019TC005596

Devoti, R., D'Agostino, N., Serpelloni, E., Pietrantonio, G., Riguzzi, F., Avallone, A., et al. (2017). A combined velocity field of the Mediterranean region. *Annals of Geophysics*, *60*(2), 0215. https://doi.org/10.4401/ag-7059

Devoti, R., Esposito, A., Pietrantonio, G., Pisani, A. R., & Riguzzi, F. (2011). Evidence of large scale deformation patterns from GPS data in the Italian subduction boundary. *Earth and Planetary Science Letters*, *311*(3–4), 230–241. https://doi.org/10.1016/j.epsl.2011.09.034

Devoti, R., Riguzzi, F., Cuffaro, M., & Doglioni, C. (2008). New GPS constraints on the kinematics of the Apennines subduction. *Earth and Planetary Science Letters*, *273*(1–2), 163–174. https://doi.org/10.1016/j.epsl.2008.06.031

Doglioni, C. (1991). A proposal of kinematic modelling for W-dipping subductions–Possible applications to the Tyrrhenian–Apennines system. *Terra Nova*, *3*(4), 423–434. https://doi.org/10.1111/j.1365-3121.1991.tb00172.x

Doglioni, C., D'Agostino, N., & Mariotti, G. (1998). Normal faulting versus regional subsidence and sedimentation rate. *Marine and Petroleum Geology*, *15*, 737–750. https://doi.org/10.1016/S0264-8172(98)00052-X

Ercoli, M., Forte, E., Porreca, M., Carbonell, R., Pauselli, C., Minelli, G., & Barchi, M. R. (2020). Using seismic attributes in seismotectonic research: An application to the Norcia Mw = 6.5 earthquake (30 October 2016) in central Italy. *Solid Earth*, *11*, 329–348. https://doi.org/10.5194/se-11-329-2020

Everett, M. E. (2013). *Near-surface applied geophysics*. Cambridge University Press.

Faure Walker, J. P., Roberts, G. P., Sammonds, P.R., & Cowie, P. (2010). Comparison of earthquake strain rates over 10^2 to 10^4 year timescales: Insights into variability in the seismic cycle in the central Apennines, Italy. *Journal of Geophysical Research*, *115*, B10418. https://doi.org/10.1029/2009JB006462

Galadini, F., & Galli, P. (2000). Active tectonics in the central Apennines (Italy) - Input data for seismic hazard assessment. *Natural Hazards*, *22*, 225–268. https://doi.org/10.1023/A:1008149531980

Galadini, F., & Galli, P. (2003). Paleoseismology of silent faults in the central Apennines (Italy): The Mt. Vettore and Laga Mts. Faults. *Annals of Geophysics*, *46*(5), 815–836. https://doi.org/10.4401/ag-3457

Gallen, S. F., & Wegmann, K. W. (2017). River profile response to normal fault growth and linkage: An example from the Hellenic forearc of south-central Crete, Greece. *Earth Surface Dynamics*, *5*, 161–186. https://doi.org/10.5194/esurf-5-161-2017

Galli, P., Ciaccio, B., Messina, P., Peronace, E., Amato, V., Naso, G., et al. (2017). Middle to Late Pleistocene activity of the northern Matese fault system (southern Apennines, Italy). *Tectonophysics*, *699*, 61–81. https://doi.org/10.1016/j.tecto.2017.01.007

Galli, P., Galadini, F., & Pantosti, D. (2008). Twenty years of paleoseismology in Italy. *Earth-Science Reviews*, *88*(1), 89–117. https://doi.org/10.1016/j.earscirev.2008.01.001

Galli, P., Galderisi, A., Peronace, E., Giaccio, B., Hajdas, I., Messina, P., et al. (2019). The awakening of the dormant Mount Vettore fault (2016 central Italy earthquake, Mw 6.6): Paleoseismic clues on its millennial silences. *Tectonics*, *38*, 687–705. https://doi.org/10.1029/2018TC005326

Gawthorpe, R. L., & Leeder, M. R. (2000). Tectono-sedimentary evolution of active extensional basins. *Basin Research*, *12*, 195–218. https://doi.org/10.1111/j.1365-2117.2000.00121.x

Geomineraria Nazionale (1963). Il bacino di Castelluccio di Norcia. In *Ligniti e Torbe dell'Italia continentale* (pp. 207–210), Industria Libraria Tipografica Editrice (ILTE).

Geurts, A. H., Cowie, P. A., Duclaux, G., Gawthorpe, R. L., Huismans, R. S., Pedersen, V. K., & Wedmore, L. J. N. (2018). Drainage integration and sediment dispersal in active continental rifts: A numerical modelling study of the central Italian Apennines. *Basin Research*, *30*, 965–989. https://doi.org/10.1111/bre.12289

Giaccio, B., Leicher, N., Mannella, G., Monaco, L., Regattieri, R., Wagner, B., et al. (2019). Extending the tephra and palaeoenvironmental record of the Central Mediterranean back to 430 ka: A new core from Fucino Basin, central Italy. *Quaternary Science Reviews*, *225*, 106003. https://doi.org/10.1016/j.quascirev.2019.106003

Giraudi, C. (2015). The upper Pleistocene deglaciation on the Apennines (peninsular Italy). *Cuadernos de investigación geográfica*, *41*(2), 337–358. https://doi.org/10.18172/cig.2696

Giraudi, C., Bodrato, G., Ricci Lucchi, M., Cipriani, N., Villa, I. M., Giaccio, B., & Zuppi, G. M., (2011). Middle to late Pleistocene glaciations in the Campo Felice basin (central Apennines, Italy). *Quaternary Research*, *75*, 219–230.

Gulunay, N. (1986). F-X Decon and the Complex Wiener Prediction Filter for Random Noise Reduction on Stacked Data. In: *56th SEG Annual International Meeting*.

Henza, A. A., Withjack, M. O., & Schlische, R. W. (2010). Normal-fault development during two phases of non-coaxial extension: An experimental study. *Journal of Structural Geology*, *32*, 1656–1667. https://doi.org/10.1016/j.jsg.2009.07.007

Henza, A. A., Withjack, M. O., & Schlische, R. W. (2011). How do the properties of a preexisting normal-fault population influence fault development during a subsequent phase of extension? *Journal of Structural Geology*, *33*, 1312–1324. https://doi.org/10.1016/j.jsg.2011.06.010

Hodge, M., Fagereng, A., & Biggs, J. (2018). The role of coseismic Coulomb stress changes in shaping the hard link between normal fault segments. *Journal of Geophysical Research, Solid Earth*, *123*, 797–814. https://doi.org/10.1002/2017JB014927

Improta, L., & Bruno, P. P. (2007). Combining seismic reflection with multifold wide aperture profiling: An effective strategy for high-resolution shallow imaging of active faults. *Geophysical Research Letters*, *34*, L20310. https://doi.org/10.1029/2007GL031893

Improta, L., Latorre, D., Margheriti, L., Nardi, A., Marchetti, A., Lombardi, A. M., et al. (2019). Multi-segment rupture of the 2016 Amatrice-Visso-Norcia seismic sequence (central Italy) constrained by the first high-quality catalog of Early Aftershocks. *Scientific Reports*, *9*, 6921. https://doi.org/10.1038/s41598-019-43393-2

Improta, L., Villani, F., Bruno, P. P., Castiello, A., De Rosa, D., Varriale, F., et al. (2012). High-resolution controlled-source seismic tomography across the Middle Aterno basin in the epicentral area of the 2009, Mw 6.3, L'Aquila earthquake (central Apennines, Italy). *Italian Journal of Geosciences*, *131*(3), 373–388. https://doi.org/10.3301/IJG.2011.35

Improta, L., Zollo, A., Herrero, A., Frattini, M., Virieux, J., & Dell'Aversana, P. (2002). Seismic imaging of complex structures by non-linear traveltime inversion of dense wide-angle data: Application to a thrust belt. *Geophysical Journal International*, *151*, 264–278. https://doi.org/10.1046/j.1365-246X.2002.01768.x

Latorre, D., Mirabella, F., Chiaraluce, L., Trippetta, F., & Lomax, A. (2016). Assessment of earthquake locations in 3-D deterministic velocity models: A case study from the Altotiberina near fault observatory (Italy). *Journal of Geophysical Research: Solid Earth*, *121*, 8113–8135. https://doi.org/10.1002/2016JB013170

Lavecchia, G., Brozzetti, F., Barchi, M., Menichetti, M., & Keller, J. V. A. (1994). Seismotectonic zoning in east-central Italy deduced from an analysis of the Neogene to present deformations and related stress fields. *The Geological Society of America Bulletin*, *106*, 1107–1120. https://doi.org/10.1130/0016-7606(1994)106<1107:szieci>2.3.co;2

Lawton, D.C. (1989). Computation of refraction static corrections using first-break traveltime differences. *Geophysics*, *54*, 1289–1296. https://doi.org/10.1190/1.1442588

Macrì, P., Smedile, A., Speranza, F., Sagnotti, L., Porreca, M., Mochales, T., & Russo Ermolli, E. (2016). Analysis of a 150m sediment core from the co-seismic subsidence depocenter of the 2009 Mw=6.1 L'Aquila earthquake (Italy): Implications for Holocene-Pleistocene tectonic subsidence rates and for the age of the seismogenic Paganica fault system. *Tectonophysics*, *687*, 180–194. https://doi.org/10.1016/j.tecto.2016.09.004

Maerten, L., Gillespie, P., & Pollard, D. D. (2002). Effects of local stress perturbation on secondary fault development. *Journal of Structural Geology*, *24*, 145–153. https://doi.org/10.1016/s0191-8141(01)00054-2

Manighetti, I., King, G. C. P., Gaudemer, Y., Scholz, C. H., & Doubre, C. (2001). Slip accumulation and lateral propagation of active normal faults in Afar. *Journal of Geophysical Research*, *106*(B7), 13667–13696. https://doi.org/10.1029/2000JB900471

Mann, J., Jäger, R., Müller, T., Höcht, G., & Hubral, P. (1999). Common-reflection-surface stack—A real data example. *Journal of Applied Geophysics*, *42*(3), 301–318. https://doi.org/10.1016/s0926-9851(99)00042-7

Maraio, S., Bruno, P. P. G., Picotti, V., Mair, V., & Brardinoni, F. (2018). High-resolution seismic imaging of debris-flow fans, alluvial valley fills and hosting bedrock geometry in Vinschgau/Val Venosta, Eastern Italian Alps. *Journal of Applied Geophysics*, *157*, 61–72. https://doi.org/10.1016/j.jappgeo.2018.07.001

Mattson, A. (2004). Tomographic imaging of late Quaternary faulting, Oquirrh Mountains, Utah. *Journal of Geophysical Research*, *109*(B11). https://doi.org/10.1029/2004JB003159

McGrath, A. G., & Davison, I. I. (1995). Damage zone geometry around fault tips. *Journal of Structural Geology*, *17*(7), 1011–1024. https://doi.org/10.1016/0191-8141(94)00116-h

Meyer, V., Nicol, A., Childs, C., Walsh, J. J., & Watterson, J. (2002). Progressive localization of strain during the evolution of normal fault systems. *Journal of Structural Geology*, *24*, 1215–1231. https://doi.org/10.1016/S0191-8141(01)00104-3

Michele, M., Chiaraluce, L., Di Stefano, R., & Waldhauser, F. (2020). Fine-scale structure of the 2016–2017 Central Italy seismic sequence from data recorded at the Italian National Network. *Journal of Geophysical Research: Solid Earth*, *125*, e2019JB018440. https://doi.org/10.1029/2019JB018440

Mirabella, F., Barchi, M. R., & Lupattelli, A. (2008). Seismic reflection data in the Umbria Marche region: Limits and capabilities to unravel the subsurface structure in a seismically active area. *Annals of Geophysics*, *51*(2–3), 383–396. https://doi.org/10.4401/ag-3032

Montone, P., & Mariucci, M. T. (2016). The new release of the Italian contemporary stress map. *Geophysical Journal International*, *205*(3), 1525–1531. https://doi.org/10.1093/gji/ggw100

Morandi, S., & Ceragioli, E. (2002). Integrated interpretation of seismic and resistivity images across the "Val d'Agri" graben (Italy). *Annals of Geophysics*, *45*, 259–271. https://doi.org/10.4401/ag-3510

Morey, D., & Schuster, G. T. (1999). Paleoseismicity of the Oquirrh fault, Utah from shallow seismic tomography. *Geophysical Journal International*, *138*(1), 25–35. https://doi.org/10.1046/j.1365-246x.1999.00814.x

Morley, C. K. (1999). Patterns of displacement along large normal faults: Implications for basin evolution and fault propagation, based on examples from East Africa. *American Association of Petroleum Geologists Bulletin*, *83*, 613–634. https://doi.org/10.1306/00AA9C0A-1730-11D7-8645000102C1865D

Morley, C. K. (2010). Stress re-orientation along zones of weak fabrics in rifts: An explanation for pure extension in 'oblique' rift segments? *Earth and Planetary Science Letters*, *297*(3–4), 667–673. https://doi.org/10.1016/j.epsl.2010.07.022

Morley, C. K. (2016). The impact of multiple extension events, stress rotation and inherited fabrics on normal fault geometries and evolution in the Cenozoic rift basins of Thailand. In C. Childs, R. E. Holdsworth, C. A.-L. Jackson, T. Manzocchi, J. J. Walsh, & G. Yielding (Eds.), *The geometry and growth of normal faults* (Vol. 439, pp. 439–445). Geological Society, London, Special Publications. https://doi.org/10.1144/SP439.3

Mouslopoulou, V., Walsh, J. J., & Nicol, A. (2009). Fault displacement rates on a range of timescales. *Earth and Planetary Science Letters*, *278*(3–4), 186–197. https://doi.org/10.1016/j.epsl.2008.11.031

Mustard, P. S. (1991). Normal faulting and alluvial-fan deposition, basal Windermere Tectonic Assemblage, Yukon, Canada. *GSA Bulletin*, *103*(10), 1346–1364. https://doi.org/10.1130/0016-7606(1991)103<1346:NFAAFD>2.3.CO;2

Nicol, A., Walsh, J. J., Villamor, P., Seebeck, H., & Berryman, K. R. (2010). Normal fault interactions, paleoearthquakes and growth in an active rift. *Journal of Structural Geology*, *32*(8), 1101–1113. https://doi.org/10.1016/j.jsg.2010.06.018

Nicol, A., Walsh, J. J., Watterson, J., & Underhill, J. R. (1997). Displacement rates of normal faults. *Nature*, *390*, 157–159. https://doi.org/10.1038/36548

Nixon, C. W., Bull, J. M., & Sanderson, D. J. (2014). Localized vs distributed deformation associated with the linkage history of an active normal fault, Whakatane Graben, New Zealand. *Journal of Structural Geology*, *69*, 266–280. https://doi.org/10.1016/j.jsg.2014.06.005

Nixon, C. W., Sanderson, D. J., Dee, S. J., Bull, J. M., Humpreys, R. J., & Swanson, M. H. (2014). Fault interactions and reactivation within a normal-fault network at Milne Point, Alaska. *American Association of Petroleum Geologists Bulletin*, *98*(10), 2081–2107. https://doi.org/10.1306/04301413177

Operto, S., Ravaut, C., Improta, L., Virieux, J., Herrero, A., & Dell' Aversana, P. (2004). Quantitative imaging of complex structures from dense wide-aperture seismic data by multiscale traveltime and waveform inversions: A case study. *Geophysical Prospecting*, *52*, 625–651. https://doi.org/10.1111/j.1365-2478.2004.00452.x

Osagiede, E. E., Duffy, O. B., Jackson, C. A.-L., & Wrona, T. (2014). Quantifying the growth history of seismically imaged normal faults. *Journal of Structural Geology*, *66*, 382–399. https://doi.org/10.1016/j.jsg.2014.05.021

Patacca, E., Scandone, P., Di Luzio, E., Cavinato, G. P., & Parotto, M. (2008). Structural architecture of the central Apennines: Interpretation of the CROP 11 seismic profile from the Adriatic coast to the orographic divide. *Tectonics*, *27*, TC3006. https://doi.org/10.1029/2005TC001917

Patruno, S., & Scisciani, V. (2021). Testing normal fault growth models by seismic stratigraphic architecture: The case of the Pliocene-Quaternary Fucino Basin (central Apennines, Italy). *Basin Research*, *33*, 2118–2156. https://doi.org/10.1111/bre.12551

Perouse, E., Benedetti, L., Fleury, J., Rizza, M., Puliti, I., Billant, J., et al. (2018). Coseismic slip vectors of 24 August and 30 October 2016 earthquakes in central Italy: Oblique slip and regional kinematic implications. *Tectonics*, *37*, 3760–3781. https://doi.org/10.1029/2018TC005083

Pierantoni, P. P., Deiana, G., & Galdenzi, S. (2013). Geological map of the Sibillini Mountains (Umbria-Marche Apennines, Italy). *Italian Journal of Geosciences*, *132*(3), 497–520. https://doi.org/10.3301/IJG.2013.08

Pizzi, A., Calamita, F., Coltorti, M., & Pieruccini, P. (2002). Quaternary normal faults, intramontane basins and seismicity in the Umbria-Marche-Abruzzi Apennine Ridge (Italy): Contribution of neotectonic analysis to seismic hazard assessment. *Bollettino Società Geologica Italiana*, *1*(1), 923–929.

Pizzi, A., Di Domenica, A., Gallovič, F., Luzi, L., & Puglia, R. (2017). Fault segmentation as constraint to the occurrence of the main shocks of the 2016 central Italy seismic sequence. *Tectonics*, *36*, 2370–2387. https://doi.org/10.1002/2017TC004652

Pizzi, A., & Galadini, F. (2009). Pre-existing cross-structures and active segmentation in the northern-central Apennines (Italy). *Tectonophysics*, *476*, 304–319. https://doi.org/10.1016/j.tecto.2009.03.018

Pizzi, A., & Scisciani, V. (2000). Methods for determining the Pleistocene–Holocene component of displacement on active faults reactivating pre-Quaternary structures: Examples from the central Apennines (Italy). *Journal of Geodynamics*, *29*(3–5), 445–457. https://doi.org/10.1016/S0264-3707(99)00053-8

Podvin, P., & Lecomte, I. (1991). Finite difference computation of travel times in very contrasted velocity model: A massively parallel approach and its associated tools. *Geophysical Journal International*, *105*, 271–284. https://doi.org/10.1111/j.1365-246X.1991.tb03461.x

Porreca, M., Fabbrizzi, A., Azzaro, S., Pucci, S., Del Rio, L., Pierantoni, P. P., et al. (2020). 3D geological reconstruction of the M. Vettore seismogenic fault system (central Apennines, Italy): Cross-cutting relationship with the M. Sibillini thrust. *Journal of Structural Geology*, *131*, 103938. https://doi.org/10.1016/j.jsg.2019.103938

Porreca, M., Minelli, G., Ercoli, M., Brobia, A., Mancinelli, P., Cruciani, F., et al. (2018). Seismic reflection profiles and subsurface geology of the area interested by the 2016–2017 earthquake sequence (Central Italy). *Tectonics*, *37*, 1116–1137. https://doi.org/10.1002/2017TC004915

Pratt, T. L., Johnson, S., Potter, C., Stephenson, W., & Finn, C. (1997). Seismic reflection images beneath Puget Sound, western Washington State: The Puget Lowland thrust sheet hypothesis. *Journal of Geophysical Research*, *102*(B12), 27469–27489. https://doi.org/10.1029/97JB01830

Pucci, S., Pizzimenti, L., Civico, R., Villani, F., Brunori, C. A., & Pantosti, D. (2021). High resolution morphometric analysis of the Cordone del Vettore normal fault scarp (2016 Central Italy Seismic Sequence): Insights into age, earthquake recurrence and throw rates. *Geomorphology*, *388*, 107784. https://doi.org/10.1016/j.geomorph.2021.107784

Pucci, S., Villani, F., Civico, R., Di Naccio, D., Porreca, M., Benedetti, L., et al. (2019). Complexity of the 2009 L'Aquila earthquake causative fault system (Abruzzi Apennines, Italy) and effects on the Middle Aterno Quaternary basin arrangement. *Quaternary Science Reviews*, *213*, 30–66. https://doi.org/10.1016/j.quascirev.2019.04.014

Puliti, I., Pizzi, A., Benedetti, L., Di Domenica, A., & Fleury, J. (2020). Comparing slip distribution of an active fault system at various timescales: Insights for the evolution of the Mt. Vettore-Mt. Bove fault system in Central Apennines. *Tectonics*, *39*, e2020TC006200. https://doi.org/10.1029/2020TC006200

Reeve, M. T., Bekk, R. E., Duffy, O. B., Jackson, C. A.-L., & Samson, E. (2015). The growth of non-collinear normal fault systems; what can we learn from 3D seismic reflection data? *Journal of Structural Geology*, *70*, 141–155. https://doi.org/10.1016/j.jsg.2014.11.007

Sapia, V., Villani, F., Lupi, M., Fischanger, F., Baccheschi, P., Brunori, C. A., et al. (2021). 3-D deep electrical resistivity tomography of the major basin related to the 2016 Mw 6.5 central Italy earthquake fault. *Tectonics*, *40*, e2020TC006628. https://doi.org/10.1029/2020TC006628

Scisciani, V., D'Intino, N., & Esestime, P. (2018). Multi-reactivated extensional domains: A case study from the Utsira High-Stord Basin (North Sea - Norway). In *Conference Proceedings, 80th EAGE Conference and exhibition 2018*. Earthdoc, European Association of Geoscientists & Engineers. https://doi.org/10.3997/2214-4609.201801517

Scisciani, V., Patruno, S., Tavarnelli, E., Calamita, F., Pace, P., & Iacopini, D. (2019). Multi-phase reactivations and inversions of Paleozoic–Mesozoic extensional basins during the Wilson cycle: Case studies from the North Sea (UK) and the Northern Apennines (Italy). *Geological Society, London, Special Publications*, *470*, 205–243. https://doi.org/10.1144/SP470-2017-232

Scognamiglio, L., Tinti, E., Casarotti, E., Pucci, S., Villani, F., Magnoni, F., et al. (2018). Complex fault geometry and rupture dynamics of the M_w 6.5, 2016, October 30th central Italy earthquake. *Journal of Geophysical Research: Solid Earth*, *123*(4), 2943–2964. https://doi.org/10.1002/2018JB015603

Silva, P. G., Goy, J. L., Zazo, C., & Bardajì, T. (2003). Fault generated mountain fronts in southeast Spain: Geomorphic assessment of tectonic and seismic activity. *Geomorphology*, *50*(1–3), 203–225. https://doi.org/10.1016/S0169-555X(02)00215-5

Stephenson, W. J., Frary, R. N., Louie, J., & Odum, J. K. (2013). Quaternary extensional growth folding beneath Reno, Nevada, imaged by urban seismic profiling. *Bulletin of the Seismological Society of America*, *103*(5), 2921–2927. https://doi.org/10.1785/0120120311

Stephenson, W. J., Odum, J. K., Williams, R. A., McBride, J. H., & Tomlison, I. (2012). Characterization of intrabasin faulting and deformation for earthquake hazards in Southern Utah Valley, Utah, from high-resolution seismic imaging. *Bulletin of the Seismological Society of America*, *102*(2), 524–540. https://doi.org/10.1785/0120110053

Stephenson, W. J., Smith, R. B., & Pelton, J. R. (1993). A high-resolution seismic reflection and gravity survey of Quaternary deformation across the Wasatch fault, Utah. *Journal of Geophysical Research*, *98*(B5), 8211–8223. https://doi.org/10.1029/92JB02873

Tan, Y. J., Waldhauser, F., Ellsworth, W. L., Zhang, M., Zhu, W., Michele, M., et al. (2021). Machine-learning-based high-resolution earthquake catalog reveals how complex fault structures were activated during the 2016–2017 Central Italy sequence. *The Seismic Record*, *1*(1), 11–19. https://doi.org/10.1785/0320210001

Tavarnelli, E. (1999). Normal faults in thrust sheets: Pre-orogenic extension, post-orogenic extension, or both? *Journal of Structural Geology*, *21*, 1011–1018. https://doi.org/10.1016/S0191-8141(99)00034-6

Taylor, S. K., Bull, J. M., Lamarche, G., & Barnes, P. M. (2004). Normal fault growth and linkage in the Whakatane Graben, New Zealand, during the last 1.3 Myr. *Journal of Geophysical Research*, *109*, B02408. https://doi.org/10.1029/2003JB002412

Vai, G. B., & Martini, I. P. (2001). *Anatomy of an orogen: The Apennines and adjacent Mediterranean basins* (p. 633). Kluwer Acad.

van Hinsbergen, D. J. J., Vissers, R. L. M., & Spakman, W. (2014). Origin and consequences of western Mediterranean subduction, rollback, and slab segmentation. *Tectonics*, *33*, 393–419. https://doi.org/10.1002/tect.2012510.1002/2013tc003349

Villani, F., Civico, R., Pucci, S., Pizzimenti, L., Nappi, R., De Martini, P. M., & The Open EMERGEO Working Group. (2018). A database of the coseismic effects following the 30 October 2016 Norcia earthquake in Central Italy. *Scientific Data*, *5*, 180049. https://doi.org/10.1038/sdata.2018.49

Villani, F., D'Amico, S., Panzera, F., Vassallo, M., Bozionelos, G., Farrugia, D., & Galea, P. (2018). Shallow high-resolution geophysical investigation along the western segment of the Victoria Lines Fault (island of Malta). *Tectonophysics*, *724–725*, 220–233. https://doi.org/10.1016/j.tecto.2018.01.010

Villani, F., Improta, L., Pucci, S., Civico, R., Bruno, P. P., & Pantosti, D. (2017). Investigating the architecture of the Paganica Fault (2009 M_w 6.1 earthquake, central Italy) by integrating high-resolution multiscale refraction tomography and detailed geological mapping. *Geophysical Journal International*, *208*(1), 403–423. https://doi.org/10.1093/gji/ggw407

Villani, F., & Pierdominici, S. (2010). Late Quaternary tectonics of the Vallo di Diano basin (southern Apennines, Italy). *Quaternary Science Reviews*, *29*, 3167–3183. https://doi.org/10.1016/j.quascirev.2010.07.003

Villani, F., Pucci, S., Civico, R., De Martini, P. M., Cinti, F. R., & Pantosti, D. (2018). Surface faulting of the 30 October 2016 Mw 6.5 central Italy earthquake: Detailed analysis of a complex coseismic rupture. *Tectonics*, *37*(10), 3378–3410. https://doi.org/10.1029/2018TC005175

Villani, F., Pucci, S., Civico, R., De Martini, P. M., Nicolosi, I., D'Ajello Caracciolo, F., et al. (2015). Imaging the structural style of an active normal fault through multidisciplinary geophysical investigation: A case study from the M_w 6.1, 2009 L'Aquila earthquake region (central Italy). *Geophysical Journal International*, *200*, 1676–1691. https://doi.org/10.1093/gji/ggu462

Villani, F., & Sapia, V. (2017). The shallow structure of a surface-rupturing fault in unconsolidated deposits from multi-scale electrical resistivity data: The 30 October 2016 M_w 6.5 central Italy earthquake case study. *Tectonophysics*, *717*(16), 628–644. https://doi.org/10.1016/j.tecto.2017.08.0010.1016/j.tecto.2017.08.001

Villani, F., Sapia, V., Baccheschi, P., Civico, R., Di Giulio, G., Vassallo, M., et al. (2019). Geometry and structure of a fault-bounded extensional basin by integrating geophysical surveys and seismic anisotropy across the 30 October 2016 M_w 6.5 earthquake fault (central Italy): The Pian Grande di Castelluccio basin. *Tectonics*, *38*, 26–48. https://doi.org/10.1029/2018TC005205

Villani, F., Tulliani, V., Sapia, V., Fierro, E., Civico, R., & Pantosti, D. (2015). Shallow subsurface imaging of the Piano di Pezza active normal fault (central Italy) by high-resolution refraction and electrical resistivity tomography coupled with time-domain electromagnetic data. *Geophysical Journal International*, *203*(3), 1482–1494. https://doi.org/10.1093/gji/ggv399

Viseras, C., Calvache, M. L., Soria, J. M., & Fernández, J. (2003). Differential features of alluvial fans controlled by tectonic or eustatic accommodation space. Examples from the Betic Cordillera, Spain. *Geomorphology*, *50*, 181–202. https://doi.org/10.1016/S0169-555X(02)00214-3

Walters, R. J., Gregory, L. C., Wedmore, L. N. J., Craig, T. J., McCaffrey, K., Wilkinson, M., et al. (2018). Dual control of fault intersections on start-stop rupture in the 2016 Central Italy seismic sequence. *Earth and Planetary Science Letters*, *500*, 1–14. https://doi.org/10.1016/j.epsl.2018.07.043

Wessel, P., & Smith, W. H. F. (1998). New, improved version of generic mapping tools released. *Eos Trans. AGU*, *79*(47), 579. https://doi.org/10.1029/98EO00426

Whipple, K. X., & Trayler, C. R. (1996). Tectonic control of fan size: The importance of spatially variable subsidence rate. *Basin Research*, *8*, 351–366. https://doi.org/10.1046/j.1365-2117.1996.00129.x

Whittaker, A. C., Cowie, P. A., Attal, M., Tucker, G. E., & Roberts, G. P. (2007). Contrasting transient and steady-state rivers crossing active normal faults: New field observations from the central Apennines, Italy. *Basin Research*, *19*, 529–556. https://doi.org/10.1111/j.1365-2117.2007.00337.x

Wilkinson, M. W., McCaffrey, K. J. W., Jones, R. R., Roberts, G. P., Holdsworth, R. E., Gregory, L. C., et al. (2017). Near-field fault slip of the 2016 Vettore Mw 6.6 earthquake (Central Italy) measured using low-cost GNSS. *Scientific Reports*, *7*, 4612. https://doi.org/10.1038/s41598-017-04917-w

Williamson, P. R., & Worthington, M. H. (1993). Resolution limits in ray tomography due to wave behaviour: Numerical experiments. *Geophysics*, *58*(5), 727–735. https://doi.org/10.1190/1.1443457

Yilmaz, O. (2001). *Seismic Data Analysis*, (2 Volumes), Society of Exploration Geophysicists. *SEG Investigations in Geophysics*, *10*, 1000.

References From the Supporting Information

Cavinato, G. P., & De Celles, P. G. (1999). Extensional basins in the tectonically bimodal central Apennines fold-thrust belt, Italy: Response to corner flow above a subducting slab in retrograde motion. *Geology*, *27*(10), 955–958. https://doi.org/10.1130/0091-7613(1999)027<0955:EBITTB>2.3.CO;2

Improta, L., Zollo, A., Bruno, P. P., Herrero, A., & Villani, F. (2003). High resolution seismic tomography across the 1980 (Ms 6.9) Southern Italy earthquake fault scarp. *Geophysical Research Letters*, *30*, 10–n. https://doi.org/10.1029/2003GL017077